Controls of River Dynamics on Residence Time and Biogeochemical Reactions of Hydrological Exchange Flows in A Regulated River Reach

Xuehang Song[1], Xingyuan Chen[1,*], John M. Zachara[1], Jesus D. Gomez-Velez[2], Pin Shuai[1], Huiying Ren[1,] and Glenn E. Hammond[3]
[1]Pacific Northwest National Laboratory, Richland, Washington, USA.
[2]Civil & Environmental Engineering, Vanderbilt University, Nashville, Tennessee, USA.
[3]Applied Systems Analysis and Research, Sandia National Laboratories, Albuquerque, New Mexico, USA.

[*]Corresponding author: xingyuan.chen@pnnl.gov; Phone: (509) 371-7510; Fax: (509) 375-2999

Keywords: Residence Time Distributions, Hydrological Exchange Zone, Hydropeaking, Biogeochemical reaction, Dam Operation, Surface water-groundwater interactions

Abstract:
Residence Time Distributions (RTDs) exerts an important control on biogeochemical translations in watershed systems. RTDs tend to follow time-invariant exponential, lognormal, or heavy-tailed RTDs that have power-law behaviors for long tails in headwater or low-order streams. However, there is increasing recognition that RTDs can be more complicated and time-variable in response to dynamic hydrological forcing. In this study, we use particle tracking to estimate RTDs along the Hanford Reach of the Columbia River and to quantify the influences of river stage fluctuations on RTDs and biogeochemical reaction potentials. Particle tracking is conducted using the velocity fields from high-resolution three-dimensional groundwater flow simulations. The effects of dynamic hydrological forcing on the RTDs were evaluated by applying time-varying river flow boundary conditions and continuously releasing particles in different time windows. Our results revealed that dynamic stage fluctuations created rapidly changing losing-gaining conditions in the river, which led to highly transient RTDs and resulted in multiple modes of RTDs. Dam-induced high-frequency (sub-daily) flow variations increased the fraction of short (sub-daily) residence times of the RTDs. Deviation of the reactant consumption under the single-mode assumption compared to the multimodal RTDs was relatively small (~5%) and the maximum deviation appeared when the Damköhler number was close to one. Dam-induced high-frequency stage variations potentially increase the biogeochemical reactions by 27%. These findings suggest that current large-scale hydrobiogeochemical models (reach to basin scales) could be improved by accounting for dynamic hydrologic exchange flows and associated transient RTDs influenced by both short- and long-term river stage fluctuations.

1. Introduction

The hydrologic exchanges between river water and groundwater play an important role in river ecosystems as the groundwater-river water mixing supplies nutrients and substrates that drive biogeochemical reactions (Boano et al., 2014; Cardenas, 2015; Gomez-Velez et al., 2015). Hydrologic exchange flows (HEFs) are defined as the vertical and lateral exchanges of water between groundwater and river water, including hyporheic exchange, bank storage, and overbank flow onto floodplains (Harvey et al., 2018; Harvey & Gooseff, 2015). HEFs span a broad range of spatial scales from millimeters to kilometers and time scales from seconds to tens of years (Boano et al., 2014; Wörman et al., 2007). The biogeochemical consequences of the HEFs depend on the residence time of the river water in the exchange zone relative to the characteristic biogeochemical time scales (BTSs), which are the intrinsic time scales of given reactions (Gomez-Velez et al., 2012).

The residence time distributions (RTDs) can be measured either through stream tracer experiments or from numerical simulations (Boano et al., 2014). RTD has been widely used as a master variable to evaluate the bigeochemical potential of the groundwater-river water mixing (Boano et al., 2010; Briggs et al., 2014; Gomez-Velez et al., 2015; Harvey et al., 2013; Zarnetske et al., 2011). RTDs tend to follow time-invariant exponential, lognormal or power-law distributions under steady flow conditions or small stage fluctuations in low-order streams (Aubeneau et al., 2015; Cardenas, 2008; Faulkner et al., 2012; Haggerty et al., 2002; Jonsson et al., 2003; Knapp et al., 2017; Sawyer & Cardenas, 2009; Tonina & Buffington, 2011; Worman et al., 2002). However, recent modeling studies demonstrated that transient RTDs may result from dynamic hydrologic conditions (Gomez-Velez & Wilson, 2013; Harman et al., 2016; Schmadel et al., 2017; Ward et al., 2018). Transient RTDs reflect the complex influences from one or multiple discrete hydrologic events that occur at different time scales with various magnitudes (McCallum & Shanafield, 2016). Even short-term perturbations (e.g., flooding) can have long-lasting influences (Gomez-Velez et al., 2017).

The shapes of RTDs in real dynamic river corridors can be very complex since RTDs are influenced by both subsurface physical features and hydrologic forcings (Boulton et al., 1998; Gomez & Wilson, 2013), including sediment permeability and porosity (Cardenas et al., 2004; Liu & Chui, 2018; Salehin et al., 2004), river morphology (e.g., riffles, bars, and dunes) (Buffington & Tonina, 2009; Cardenas, 2008; Cardenas & Wilson, 2007; Stonedahl et al., 2013), naturally occurring hydrologic processes and events (e.g., flooding, evapotranspiration, recharge, snowmelt and tidal cycles) (Gomez-Velez et al., 2017; Gomez-Velez & Wilson, 2013; Larsen et al., 2014), and anthropogenic activities (e.g., dam-induced stage fluctuations) (Shuai et al., 2019; Song et al., 2018). The dynamic hydrologic fluctuations can produce equivalently complex pathways and RTDs as complex geomorphic features (Schmadel et al., 2016).

Dynamic flow variations are common in most large river systems, which exhibit multi-frequency patterns that are influenced by natural processes and anthropogenic activities (Graf, 1999; Nilsson et al., 2005). These stage variations cause significant pressure changes along the river shoreline and significant lateral exchange flow and bank storage (Shuai et al., 2019; Zachara et al., 2016), which enhance biogeochemical processes within the river corridors (Briody et al., 2016; Knapp et al., 2017; Shuai et al., 2017; Song et al., 2018; Trauth & Fleckenstein, 2017). However, there have been few studies that link HEFs, RTDs and their biogeochemical consequences within large river corridors due to challenges in data collection and lack of modeling capability (Boano et al., 2014). The traditional tracer experiment methods [e.g., (Knapp et al., 2017; Worman et al., 2002)] mainly work for low-order small streams. Numerical methods such as particle tracking (Cardenas et al., 2004; Faulkner et al., 2012), time-derivative of solute breakthrough curves (Cardenas, 2008), or the StorAge Selection (SAS) function (Botter et al., 2011; Rinaldo et al., 2015) are often data-intensive and/or computationally expensive.

In this study, we explore three questions: (1) what are the characteristics of RTDs under dynamic river flow conditions induced by dam operations? (2) how do the resulting RTDs impact biogeochemical

reactivity in the exchange zone? and 3) can we provide some general guidance on evaluating the impacts of HEFs on biogeochemical cycling in large dynamic river systems? To resolve these questions, we estimated RTDs by conducting particle tracking using multi-year velocity outputs from km-scale, 3D groundwater flow and transport models. The simulated RTDs were then used to evaluate the impacts of river dynamics on generalized river corridor biogeochemical reactions. We chose the Hanford Reach of the Columbia River as an example in this study, which serves as an ideal testbed because of its highly dynamic HEFs (Shuai et al., 2019; Song et al., 2018). In addition, extensive hydrologic and geologic data collected from more than thirty monitoring wells within this site provides detailed site characteristics. The general approaches of this study can be extended to other study sites. Our study improves the understanding of the influences of dynamic flow conditions on RTDs, and their biogeochemical reaction potential associated with groundwater-surface water exchange.

2. Materials and Methodology

We used particle tracking to evaluate the RTDs of intruded river water in the aquifer. The particle tracking was conducted based on velocity fields simulated by a high-resolution 3D groundwater model with in-situ groundwater montoring data. Particles were injected at multiple locations in the river-aquifer interface under various river flow conditions to account for the spatial/temporal variations of RTDs. We then adopted a first-order kinetics equation to quantify the impacts of RTDs on typical biogeochemical reactions expected to occur within river corridors. In addition, a second case with daily smoothed flow boundaries was compared to the base case to evaluate the influence of dam-induced, high-frequency flow variations.

2.1 Site Description

The study area is situated near the downstream end of the Hanford Reach of the Columbia River, located within the semi-arid Pasco Basin in southeastern Washington State (Figure 1). The Hanford Reach is an 80 km free-flowing river segment bounded by two hydroelectric dams, including the upstream Priest Rapids Dam and the downstream McNary Dam (Neitzel et al., 2001). Dam operations for power generation and seasonal snow melting strongly impact the river discharge, leading to river stage fluctuation up to 2 m daily and 4-5 m annually (Arntzen et al., 2006). Numerous groundwater wells were installed as part of the Hanford remediation efforts for monitoring groundwater level, temperature and chemistry data (Bjornstad et al., 2009). A river routing model, the Modular Aquatic Simulation System in 1-Dimension (MASS1), has been well calibrated against river gauge observations with mean absolute error ranging from 4 to 18 cm (Richmond & Perkins, 2009), which provided accurate river stage and gradient information along the reach.

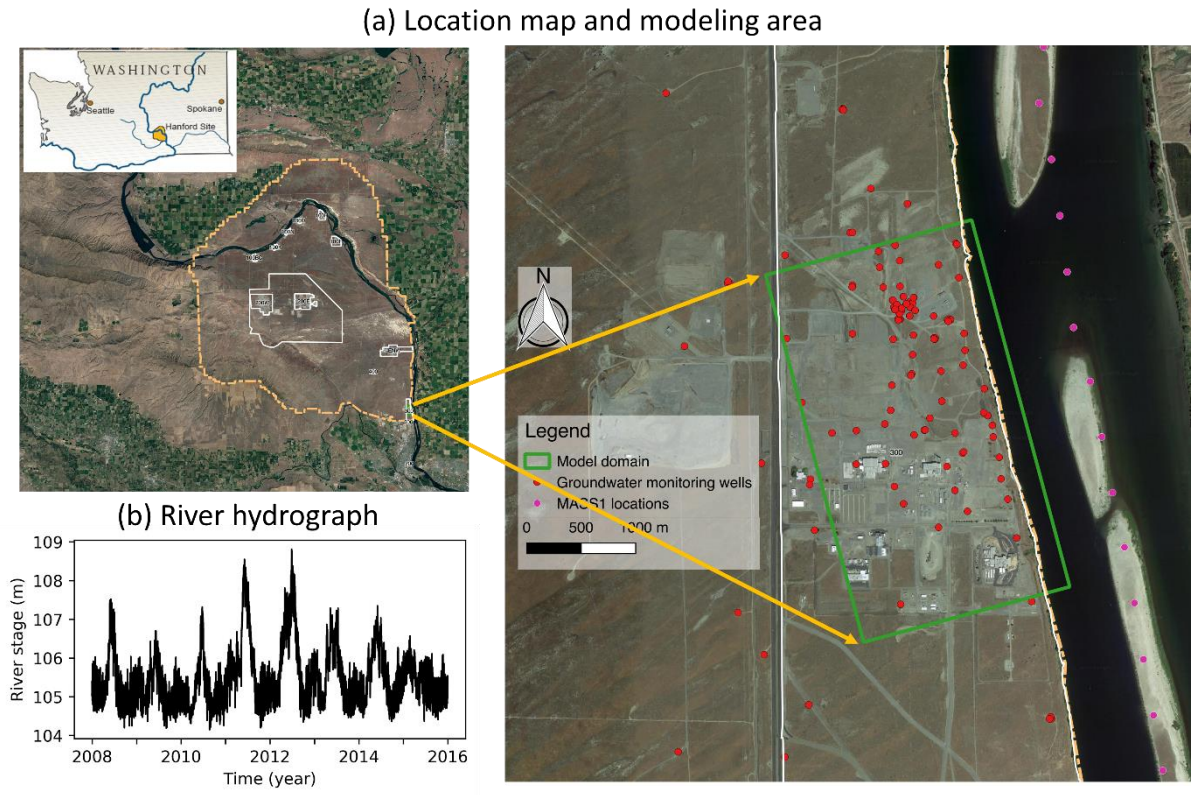

Figure 1. (a) Location map and modeling area. The red dots represent the groundwater monitoring/sampling wells, the purple dots represent MASS1 transects, and the green box shows the groundwater model domain; (b) river hydrograph between 2008 and 2015.

The unconfined aquifer within the river corridor consists of two major geologic formations including the upper high-permeability Hanford Formation, consisting of coarse gravelly sand and sandy gravel; and the lower, low-permeability Ringold Formation composed primarily of silt and fine sand (Bjornstad et al., 2009; Chen et al., 2012, 2013; Williams et al., 2008; Zachara et al., 2013, 2016). The aquifer-river interface is comprised of a low-permeability sandy layer of recent fluvial deposition. The thin alluvium layer (0.5m~2m) has an important influence on HEFs by dampening river fluctuation propagation into the aquifer (Hammond & Lichtner, 2010; Song et al., 2018; Zhou et al., 2018).

2.2 Flow and Transport Model

3-D groundwater flow and transport models were built to simulate the transient flow field and river intrusion using the massively parallel subsurface flow and reactive transport code PFLOTRAN (pflotran.org) (Hammond et al., 2014). The governing flow equation in PFLOTRAN is the Richards equation. The dominant solute transport mechanisms in this site are advection and macro-dispersion due to the dynamic flow conditions and the structurally heterogeneous, high-permeability aquifer, while molecular diffusion is neglected. The governing equations for flow and solute transport are included in the Supporting Information (S1).

A 1600x900x20 m model domain (the green box in Figure 1) was selected to encapsulate a known paleochannel within the Hanford 300 Area. More than 30, long-term monitoring wells exist within the domain to monitor the attenuation of a persistent uranium plume. The grid size was 4 m horizontally and 0.5 m vertically, with a total of 3.6 million grid cells. Groundwater flow and transport simulations were performed for an eight-year time window (2008-2015), with the first year used for model spin-up and the

other seven years used for conducting particle tracking. The maximum time step in this simulation was set to one hour, while PFLOTRAN refines the time step to achieve convergence when needed.

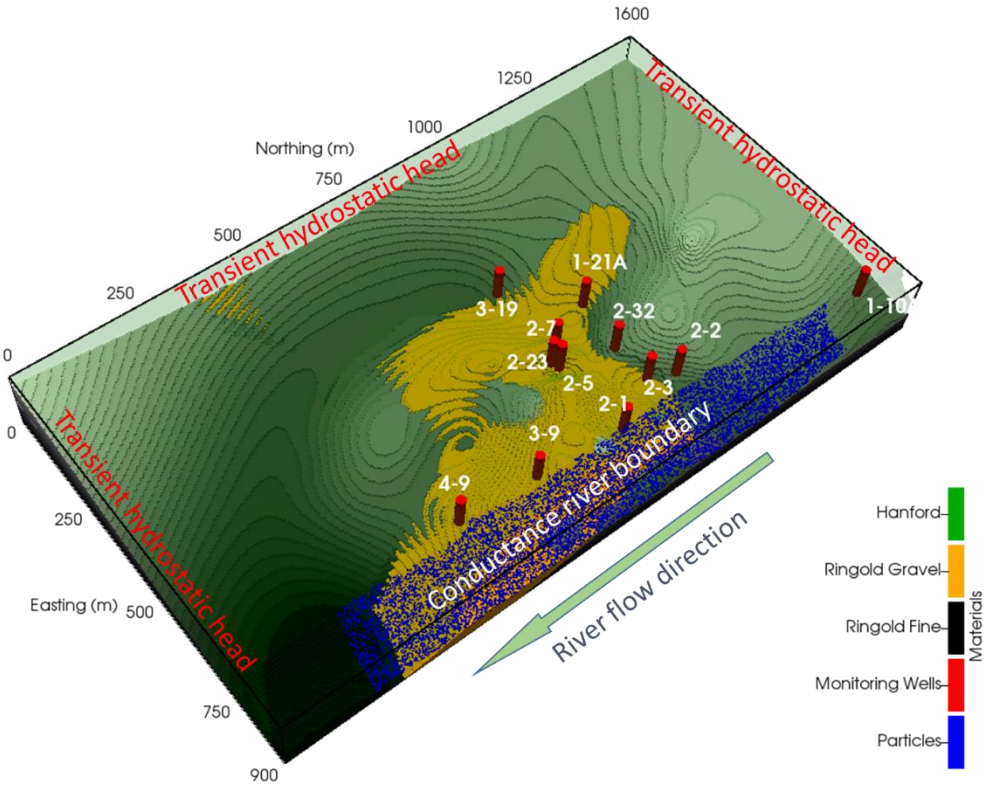

Figure 2. Model domain. The upper Hanford Gravel (green) is set translucent to show the lower Ringold Fines (black to grey) and Ringold Gravel (orange). The red cylinders represent the long-term monitoring groundwater wells used for model validation. The blue dots indicate particle release locations.

Three distinct hydrogeological units were delineated from the Hanford and Ringold Formations for the 3D model (Figure 2), including the Hanford Gravel (HG), Ringold Fines (RF), and Ringold Gravel (RG). The hydraulic properties were modified from earlier modeling studies performed at the site (Chen et al., 2013; Song et al., 2018) as listed in Table 1. The permeability field was assumed to be homogeneous within each unit with vertical permeability as one-tenth of horizontal permeability. Because the actual thickness of the alluvium layer is unknown (0.5m~2m) and unlikely to be accurately represented by the model resolution (4×4×0.5 m), a conductance boundary condition was applied at the river-sediment interface (Hammond & Lichtner, 2010). Four different conductance coefficient values were applied to the river boundary to find the best fit for monitored groundwater elevation and chemical data. A conductance coefficient of 2.5×10^{-13} m was chosen after comparing simulated tracer breakthrough curves with observed specific conductance in selected wells (Section 3.2). More detailed description of the conductance boundary is included in the supporting information (S1).

Table 1. Hydraulic properties of Hanford Gravel/Ringold Gravel/Ringold Fine in the flow model

	Hanford Gravel	**Ringold Gravel**	**Ringold Fine**
Horizontal permeability (m^2)	7.38×10^{-9}	$4.72e\times10^{-11}$	1.18×10^{-12}

Porosity (-)	0.2	0.25	0.43
Residual saturation (-)	0.16	0.13	0.13
van Genuchten alpha parameter (Pa^{-1})	7.27×10^{-4}	1.43×10^{-4}	1.43×10^{-4}
van Genuchten m parameter [-]	0.34	0.75	0.75

Hydraulic head along the river boundary was interpolated using the hourly river stage outputs from the river routing model MASS1 (Richmond & Perkins, 2009). The transient hydraulic head at the lateral inland (south/west/north) boundaries was kriged using groundwater level data of wells located inside and outside of the model domain. A constant-rate recharge of 55.4 mm/yr was applied on the upper model boundary based on monitoring results at nearby locations (Fayer & Walters, 1995). The bottom of the model domain was set as no-flow as it is underlain by the Ringold Formations with low permeability. The initial head over the model was kriged using the same set of data for the lateral inland boundaries. An in-silico conservative tracer with a unit concentration was continuously released along the river boundary to track river water penetrating in the aquifer. The simulated tracer concentration represents the fraction of river water in the aquifer. The transport conditions for the lateral inland boundaries were set as zero dispersive gradient for outflow and zero concentration tracer for inflow. The recharge of the top boundary contains no tracer while the lower boundary was zero flux due to the no flow condition.

A baseline groundwater flow model was built using the original MASS1 simulated river stage results with hourly resolution and hourly groundwater table monitoring data. An additional simulation with daily smoothed flow boundaries was used to evaluate the influence of dam-induced, high-frequency flow variations. Velocity fields of both baseline and smoothed models were used to drive particle tracking simulations to derive RTDs. The results of the smoothed case are discussed in section 3.6.

2.3 Particle Tracking and RTD Estimations

We use forward particle tracking to simulate the hydrological exchange pathways and estimate RTDs. We adopted a classical semi-analytical particle tracking scheme (Pollock, 1994) which tracks particles from one cell to the next until the particle reaches a model boundary or satisfies a termination criterion (e.g., particles lost in the vadose zone). Numerical particles were released from 10,000 randomly selected locations along the river shoreline at 10,000 random times during the seven-year simulation window to cover an adequate range of advection paths. Convergence tests were conducted to ensure the number of released particles were large enough to provide consistent results. Each particle was released 10^{-7} m below the riverbed as represented by the blue dots in Figure 2. More than half (67%) of the total 100 million released particles did not enter the groundwater aquifer due to local groundwater discharge conditions when they were released. Thus they were not tracked and counted in the following RTD estimation. The parallel particle tracking scheme is described in the supporting information (S2). A parallel particle tracking software package using Python was built for this study and is publicly available on Github (https://github.com/xuehangsong/particle_tracking/).

The residence time of each particle is defined as the time elapsed from entering the riverbed to exiting through the aquifer. Then the particle residence times were weighted by the fluxes corresponding to the location and time when it was released to estimate the cumulative residence time distribution (CRTD; $F_{RT}(t)$) as

$$F_{RT}(t) \approx \hat{F}_{RT}(t) = \frac{\sum_{i=1}^{N} |v_i| \cdot \mathbf{1}_{T_i \le t}}{\sum_{i=1}^{N} |v_i|}, \quad (1)$$

where $\hat{F}_{RT}(t)$ is the empirical cumulative distribution, N is the number of particles, v_i is the Darcy flux when and where the particle i is released, T_i is the particle residence time, $\mathbf{1}_{T_i \le t}$ is the indicator of event $T_i < t$. The CRTD $F_{RT}(t)$ was then used to derive the RTD $f_{RT}(t)$ as

$$f_{RT}(t) = \frac{d}{dt} F_{RT}(t) \ . \tag{2}$$

Three types of particles (<2.5%) were not included in our analysis: 1) particles released in the last month of the year 2015 as these particle paths failed to complete by the end of the simulation; 2) particles that flowed out the inland groundwater boundaries of the domain; 3) particles immobilized in the vadose zone. The overall RTD of all qualified particles represent lumped temporal and spatial variations of residence time along the modeled river reach during this nearly seven-year time period. We used the Bayesian Information Criterion (BIC) (Spiegelhalter et al., 2002) to find the best distribution model to describe the overall RTD. The BIC is a model selection criterion and the model with the lowest BIC has the best balance between goodness-of-fit and model parsimony. BIC usually first decreases then increases as more model parameters are included in the model fitting. To further distinguish the spatial and temporal variations of RTDs, we applied several moving temporal (one week, six months and one year) and spatial (5 m, 50 m and 500 m) windows to extract subsets of particles and estimate their temporally/spatially discrete RTDs.

2.4 Impacts of RTDs on Biogeochemical Reactions

We evaluated the biogeochemical impacts of the simulated RTDs by linking them to a generic biogeochemical reaction with different reaction rates. There are various formulations to describe the microbial redox kinetics in biogeochemistry literature, such as zero- and first-order kinetics, Monod, and dual-Monod kinetics depending on the number of involved reactants and the degree of mathematical complexity (Bekins et al., 1998; Boano et al., 2010). Since the solute reaction was not directly modeled in the particle tracking simulations, we adopted a simple first-order kinetics for the reactions along the exchange pathways, i.e.,

$$\frac{dC}{dt} = -k \cdot C \ , \tag{3}$$

where C is the reactant concentration, t is time and k is the first-order decay constant and defined by

$$k = 1/\tau \ , \tag{4}$$

where τ refers to the characteristic biogeochemical timescale (BTS) (Gomez-Velez et al., 2015). The ratio between the median residence time $F_{RT}^{-1}(0.5)$ and τ defines the Damköhler number as

$$D = \frac{F_{RT}^{-1}(0.5)}{\tau} \ . \tag{5}$$

The reactive transport system is regarded as mass-transfer limited and reaction rate limited when Damköhler number is larger than and smaller than one, respectively.

By integrating Eq. (3) from time 0 to t, we get

$$C(t) = C_0 \exp(-kt) \ , \tag{6}$$

where C_0 is the initial amount of reactant concentration entering the riverbed, $C(t)$ is the residual reactant concentration after river water resides in the riverbed for time t. Then the fraction of consumed reactant after t is

$$F_{solute}(t) = 1 - \frac{C(t)}{C_0} = 1 - \exp\left(-\frac{t}{\tau}\right). \quad (7)$$

$F_{solute}(t)$ represents the percentage of reactive solute that can potentially be consumed in a batch reactor given a certain BTS τ within time *t*. The simulated RTD, $p_{rtd}(t)$, represent the time distribution of reactive solute residing in the batch reactor (i.e., river bed aquifer). By integrating the product of $F_{solute}(t)$ and $p_{rtd}(t)$ over time window *t*, the percentage of total reactant consumption, P_{solute}, in the river corridor can be calculated by;

$$P_{solute} = \int_{-\infty}^{+\infty} \left[p_{rtd}(t) \times F_{solute}(t) \right] dt . \quad (8)$$

3. Results

3.1 Exchange Flow Patterns as Evidenced by Specific Conductance Measurement

The distinct contrast in river water and groundwater specific conductance (SpC) at the Hanford site makes SpC a natural tracer of river water and groundwater mixing (Stegen et al., 2018). The average groundwater SpC is ~500 uS/cm, while that of the Columbia River is ~120 uS/cm. Thus, the SpC measurements in monitoring wells decreased when river water intrudes and increased when river water retreats. The annual and seasonal variations of river water exchange patterns in the near-shore region of the flood plain aquifer are illustrated in Figure 3 using SpC fields kriged from distributed well-based monitoring data. In a typical high water year (2012, T1 in Figure 3), river water intrusion (blue color) can be ~300 meters inland and occupy almost the entire shoreline. However, during a low-water drought year (2015, T5 in Figure 3), the presence of river water was limited to some preferential flow paths near the shoreline. The maximum river water intrusion for an average flow year is shown in T3 in Figure 3. Significant seasonal variations occurred in the kriged SpC field (T2, T4, and T6 in Fall compared to T1, T3, and T5 in Spring in Figure 3), river water is barely found in the aquifer, even in the near-shore areas in late fall of each year (T2, T4, and T6 in Figure 3) due to low mean river stage and groundwater outflow under a sustained period of river stage decline.

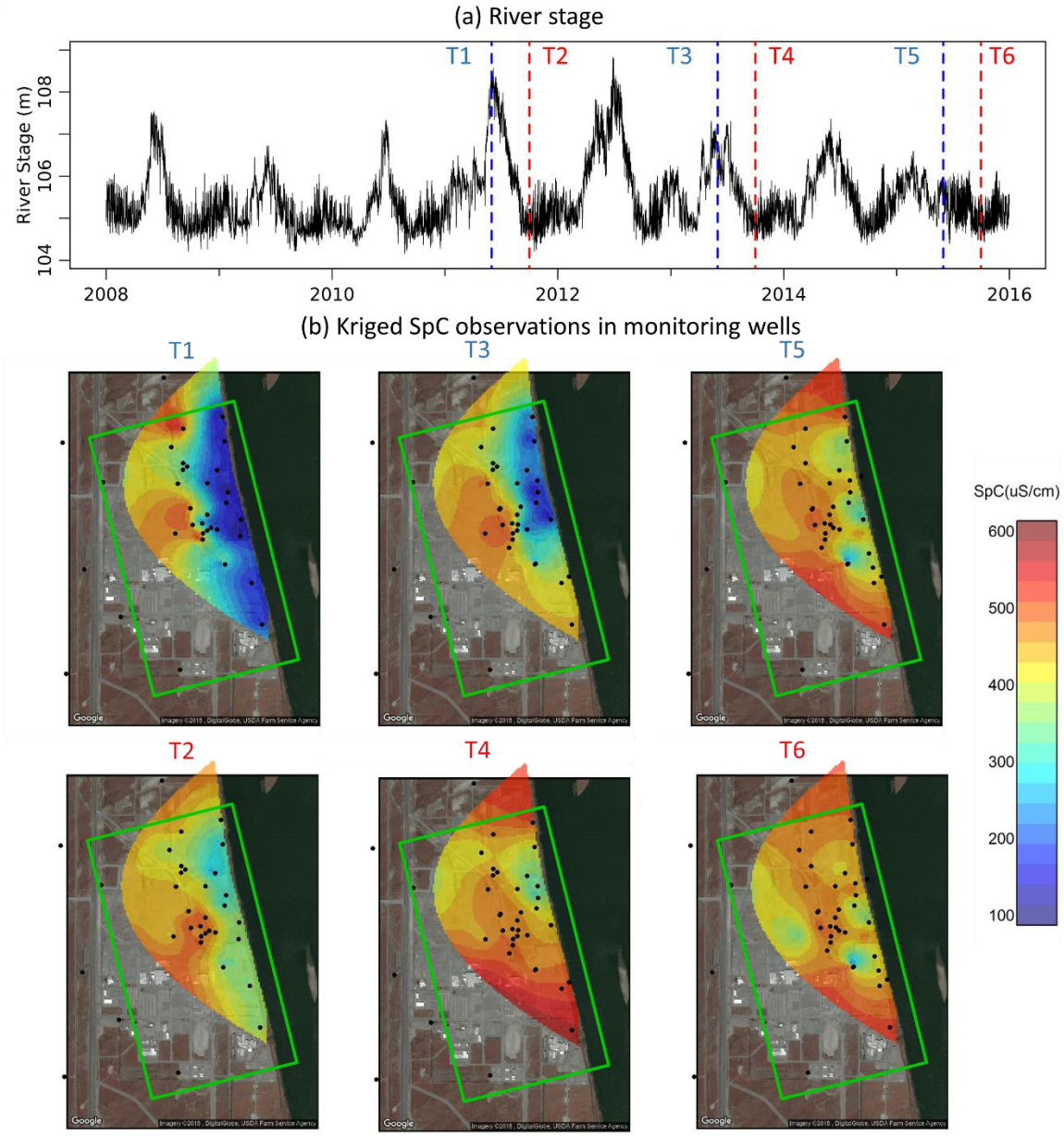

Figure 3. Observed river hydrograph (a) and snapshots of river water intrusion patterns indicted by kriged SpC maps (b). Areas with higher SpC (warm colors) have less river water presenting, while areas with lower SpC (cold colors) have more river water presenting.

3.2 Flow Model Validation

Groundwater table elevation and SpC observed in the monitoring wells were used for model validation. The simulated groundwater table elevations agreed well with the monitored water tables (supporting information S3), primarily due to the small hydraulic gradients of the highly permeable aquifer. However, the match between the simulated and observed SpC was less ideal as the local heterogeneity of flow and transport processes has more significant control on water chemistry. We link the SpC observations and simulated conservative tracer results through the concept of river water fraction, i.e., the volume fraction of river water presenting in the aquifer. The observed river water fraction ($F_{\mathrm{RW,obs}}$) was estimated by normalizing the measured SpC data as follows:

$$F_{\mathrm{RW,obs}} = \frac{\mathrm{SpC_{max}} - \mathrm{SpC_{obs}}}{\mathrm{SpC_{max}} - \mathrm{SpC_{min}}} , \quad (9)$$

where $\mathrm{SpC_{max}}$ and $\mathrm{SpC_{min}}$ were the maximum and minimum SpC observations in the groundwater well and river, respectively, and $\mathrm{SpC_{obs}}$ was the actual measured SpC value. The simulated river water fraction $F_{\mathrm{RW,simu}}$ was equal to the value of simulated tracer concentration $\mathrm{C_{simu}}$ as

$$F_{\mathrm{RW,simu}} = \frac{\mathrm{C_{simu}} - 0}{1 - 0} = \mathrm{C_{simu}} , \quad (10)$$

since the tracer is only released at river boundary with a unit concentration.

The simulated river water fractions were compared with the observed river water fractions to identify the appropriate conductance coefficient (Figure 4, shown for representative wells). Well 2-2 is a representative well in the upstream, near-shore locations, which usually have the highest river water fraction and fastest response to river elevation changes. Well 2-32 is in the middle of the well field, which is less dynamic than the near-shore wells, and experiences river water intrusion at intermediate and high river stages (>106 m). Well 1-21A is relatively far inland and only experiences significant river water intrusion around the peak flows of a high water year (>108 m). Well 4-9 is a downstream, shoreline well. The mismatch between simulated and observed river water fractions in well 4-9, a downstream shoreline well, is larger than the other wells due to the accumulated error along the upgradient flows from north to south and west to east,. The match between observation and simulation was deemed quite satisfactory with the conductance value of $2.5e{\times}10^{-3}$ m given our assumption of homogenous hydraulic properties in each hydrogeological unit. The match can be further improved in the future by incorporating more field surveys and characterizing local heterogeneity through data assimilation approaches. More information about the flow simulation results are included in supporting information (S4).

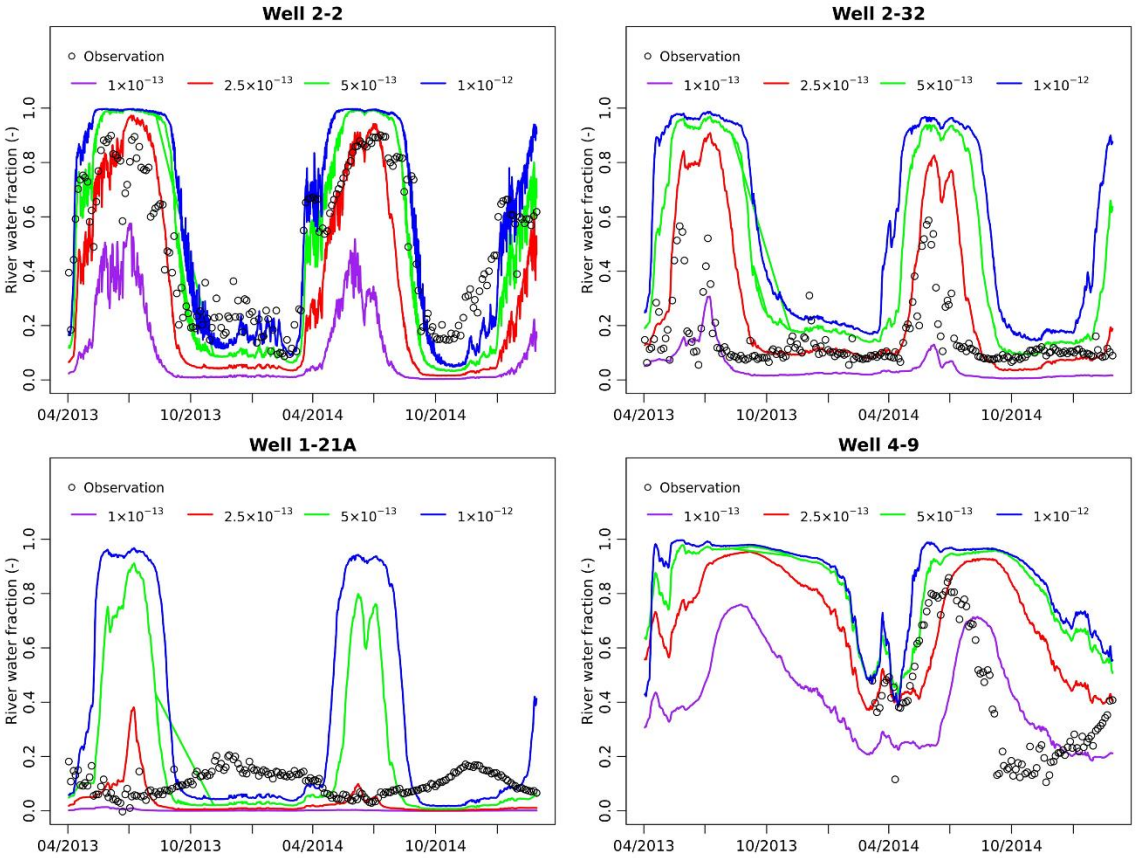

Figure 4. Comparison between modeled and observed river water fraction. The black dots are river water factions converted based on SpC observations, the colored lines are river water fractions converted from simulated river water concentrations with different conductance values.

3.3 Spatial and Temporal Variations of Exchange Pathways

The particle tracking results revealed that complex exchange pathways varying with particle release times and locations. We show in Figure 5 the seasonal and spatial variation of paths from a group of particles that were released around the elevation of 103.5m, which was chosen for illustration because it was always saturated during the 7-yr simulation window. Particles released in Jan 2009 (T1) track the exchange paths during low river stages under which the river was mainly gaining. Particles that entered the aquifer during this period were driven by short-term river fluctuations and returned to the river shortly after. Particles released in T2 exhibited dynamic, back-and-forth lateral movement that was common when there is frequent reverse of flow directions. Particles released prior to peak stage events (T3-T6) displayed the largest inland migration with longest residence time under wet (2012, T3), average (2013, T4; 2014, T5) and drought (2015, T6) conditions. The river particles released in the downstream portion were only transported tens of meters inland (T4-T6), whereas river water particles travelled hundreds of meters inland when they entered the aquifer from the upstream locations. An animation of the particle tracking results is included in the supporting information (movie S1).

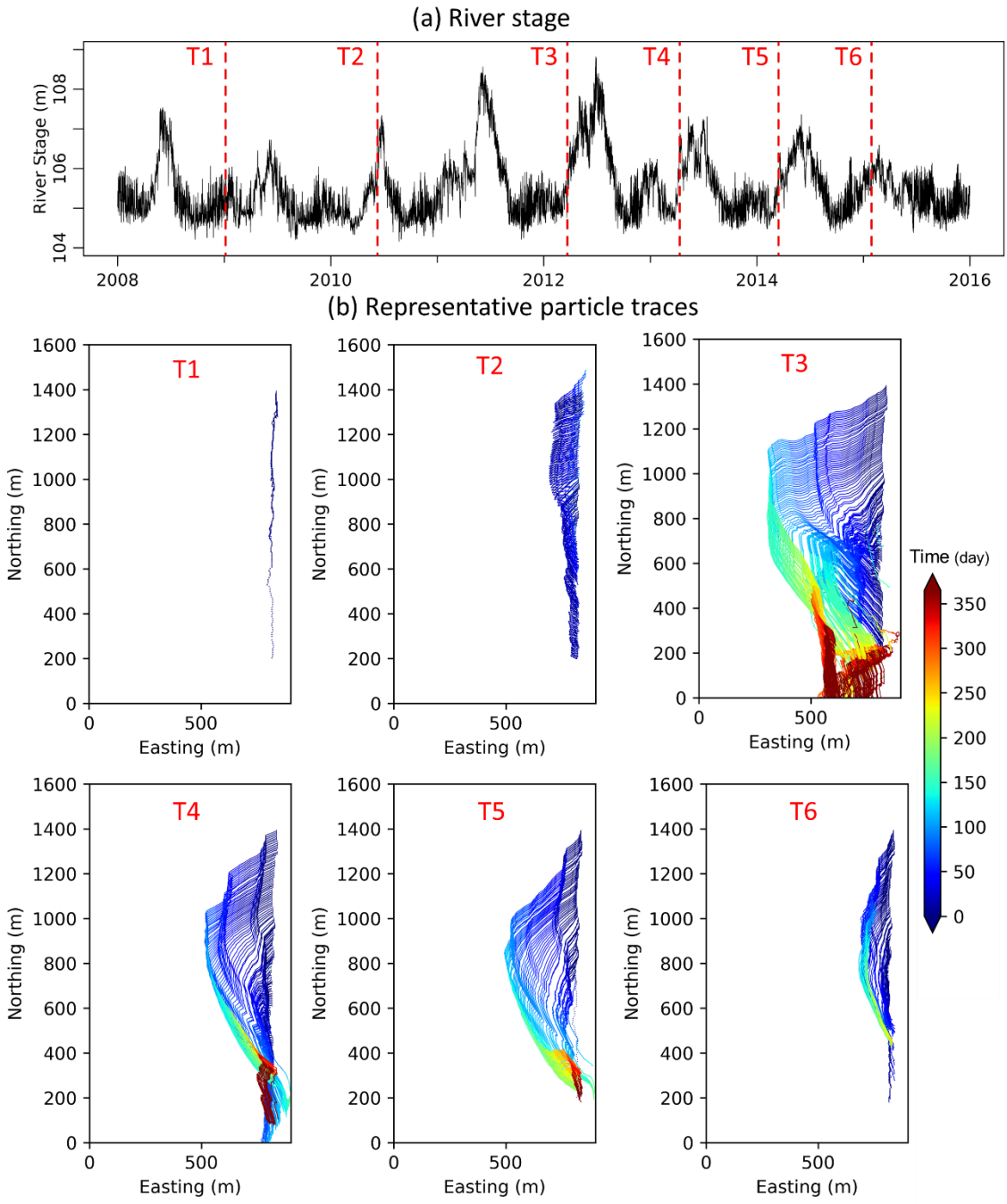

Figure 5. Flow paths of particles released at elevation of 103.5m, a) river stage time series marked with six representative release times; b) representative particle traces. The colors in (b) indicate residence time of each particle in the aquifer.

Our results revealed that more than 97% of released particles returned to the river due to the gaining river conditions. Most of the rest of the 3% particles were lost through outflow across the southern groundwater boundary under significantly low river state conditions (see T3 in Figure 5b). These particles were not included in the calculation of the RTDs, although they may eventually return to the river later in

a larger modeling domain. As a result, some particles could potentially contribute to long tails in RTDs were missing in our simulation results.

3.4 Transient and Multimodal RTDs Induced by Dynamic Flow Variations

The direction of the HEFs across the riverbed has a significant impact on the movement of river particles in the subsurface. A particle will not enter the subsurface model domain when released under gaining river conditions, hence not tracked in our algorithm. Figure 6b illustrates the distribution and direction of river exchange fluxes along the river shoreline over time. The upstream segment of the riverbed experienced more river water intrusion (red colors, Figure 6b), while the downstream segment was dominated by groundwater discharge (blue colors, Figure 6b). The subsurface stratigraphy had a significant influence on the exchange fluxes, e.g., the flux rate was 10 times lower where the less permeable Ringold Formations were present within the river stage fluctuation zone (around the middle part of the river shoreline shown in Figure 6b).

Residence times of the particles ranged from hours to years depending on the particle releasing time and location under the baseline case (Figure 6c). The blank areas in Figure 6c correspond to locations and times that groundwater discharge occurred, shown as the blue areas in Figure 6b. Particles released in the northern upstream locations tended to have longer residence times, which was consistent with their long exchange pathways shown in Figure 5.

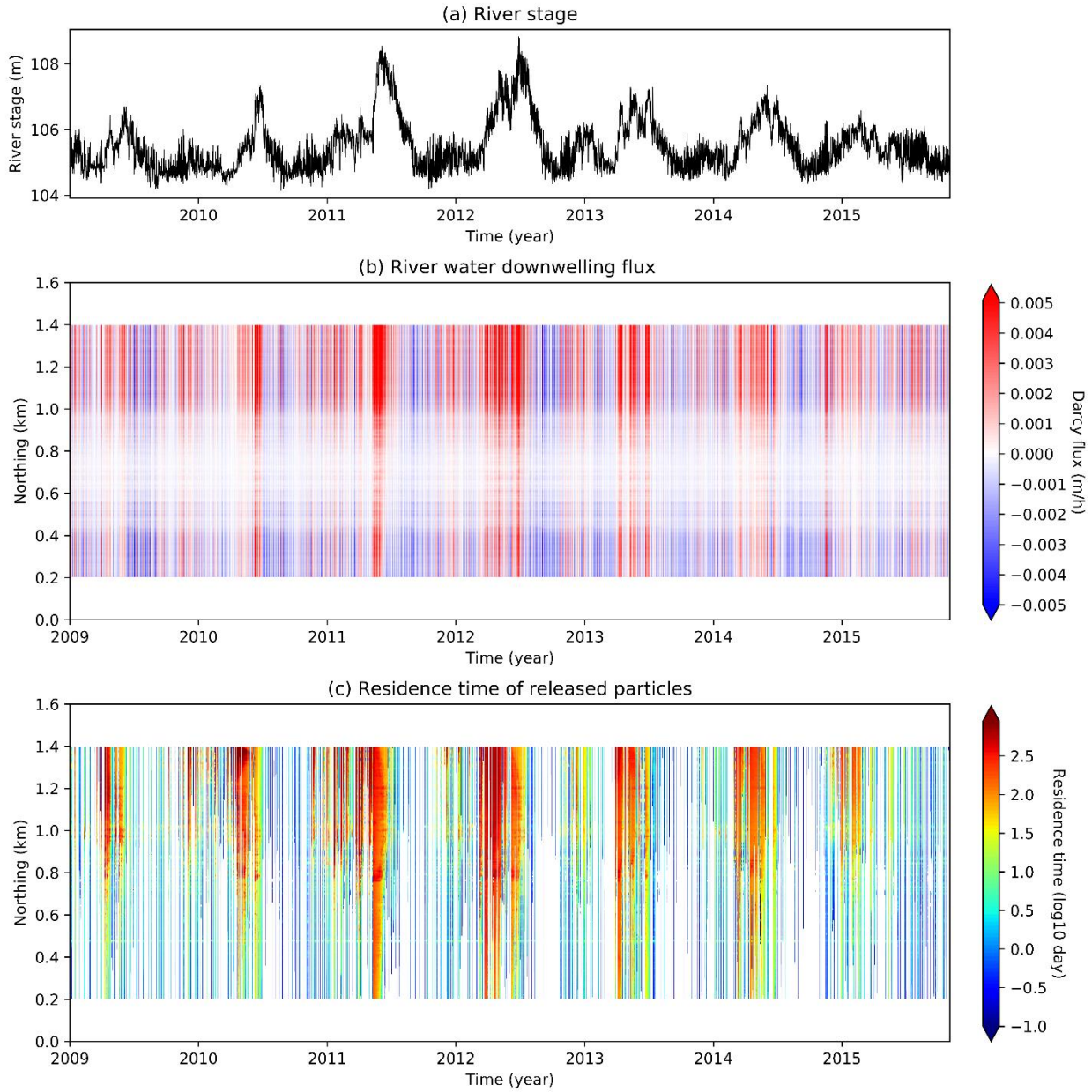

Figure 6. Time series of (a) river stage, (b) spatial/temporal distribution of the exchange flux (red colors mean river water intrusion, blue colors mean groundwater discharge) on the riverbed, and (c) spatial/temporal distribution of the river particle residence time. The blank areas in (a) are time/locations where groundwater discharge happened (the blue area in (b)).

The RTD estimated using Eq. (2) exhibited strong multimodal distributions as shown in Figure 7 (the grey shadow). Although RTDs with single-mode lognormal shapes were good representations of the advection based exchange models under steady-state flow conditions (Cardenas et al., 2004; Worman et al., 2002), our results clearly demonstrate that this assumption does not hold under highly dynamic flow conditions. The single-mode lognormal distribution (solid black line in Figure 7) could hardly fit the simulated RTD. We then used the Bayesian Information Criterion (BIC) (Spiegelhalter et al., 2002) to select an optimal number of modes that could sufficiently fit the overall RTD. However, the BIC did not converge to a minimum value even after more than 50 modes were assumed to exist in this case. Since there is negligible improvement to the BIC when the number of modes exceeds eight, we adopted an

eight-mode Gaussian Mixture Model (GMM) as our upper limit in Figure 7 (colored dash lines representing individual modes, while the black dash line represents resulted GMM).

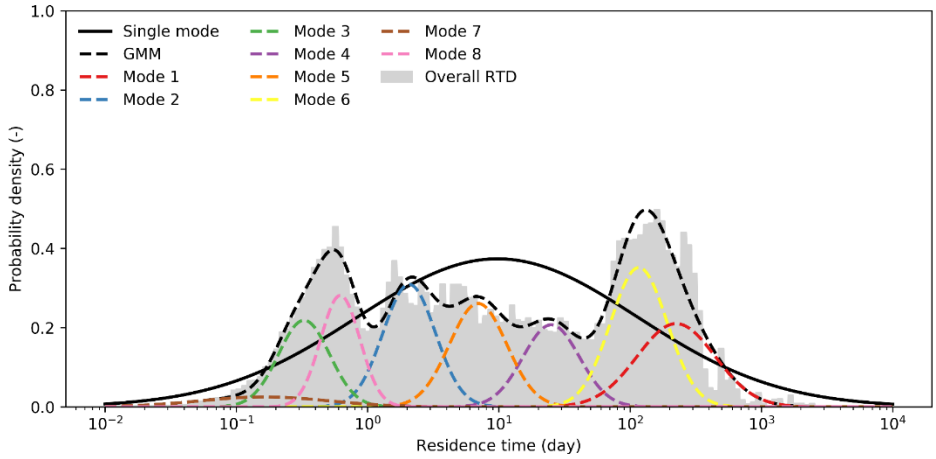

Figure 7. Overall RTD of particles released in 6-year simulation period and fitted GMM modes.

We decomposed the overall particle tracking results to smaller subsets based on their releasing times and locations to evaluate the temporal and spatial variations of RTDs. Temporally, moving windows of one week, six month and one year were chosen and their CRTDs were calculated based on Eq. (1) and plotted against the overall CRTD in Figure 8a. Longer time windows tended to yield smaller variations in their CRTDs and were closer to that of the overall CRTD as they captured river dynamics over a bigger time window. However, the variation in CRTDs using time windows of one year is still considerably large (light blue lines in Figure 8a). Similarly, spatial moving windows of 5m, 50m, and 500m were chosen to generate spatially discrete CRTDs (Figure 8b). The comparison between Figure 8a and Figure 8b show that dynamic river stage variation is the major contributor to the complex RTDs pattern, as the spatial variations in CRTDs are much smaller compared to their temporal variations, e.g. the spread of the CRTDs in 5m spatial window (dark green lines in Figure 8b) is even smaller than the spread of the CRTDs in one year time windows (light blue lines in Figure 8a). We adopted the Kolmogorov–Smirnov (K-S) tests to compare the temporal/spatial discrete RTDs with the overall RTD. All the tests were rejected with significance levels below 1%, indicating that the temporal/spatial discrete RTDs and the overall RTD did not follow the same distribution. These results suggest that it may not be possible to determine a precise shape of RTDs for a river reach with complex aquifer hydrogeological features that experiences dynamic flow conditions.

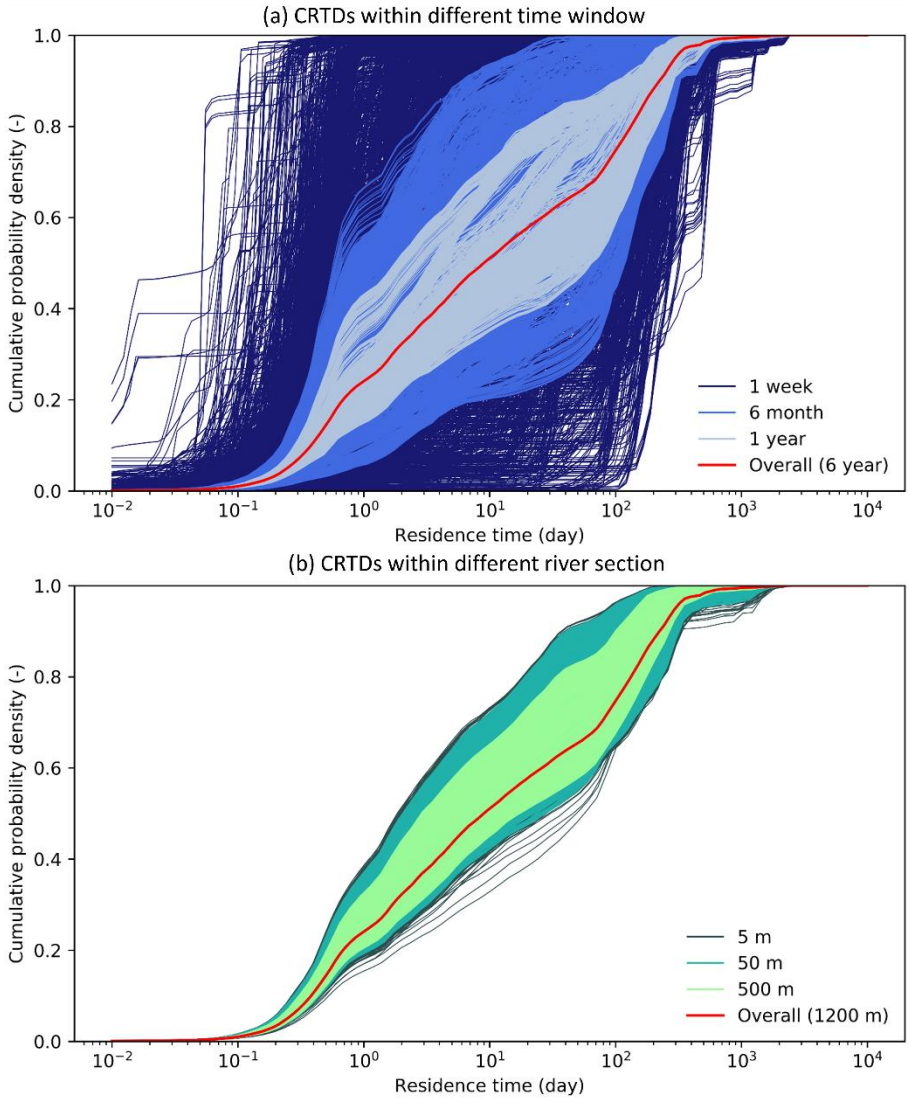

Figure 8. Estimated CRTDs of temporal (a) and spatial (b) subsets of particles. The red line is the overall CRTDs for all the eligible particles

3.5 Biogeochemical Implication of the Transient Multimodal RTDs

The consumption fractions of reactants were used to evaluate the potential biogeochemical implications of transient multimodal RTDs. The BTS (biogeochemical time scale) τ has a wide range in value depending on the microbial, geochemical, and hydrologic of sediment properties. We chose four representative BTSs at 1, 10, 100 and 1000 hours to explore its uncertainty. As a reference, the BTSs of two typical biogeochemical reactions common to river corridors, denitrification and aerobic respiration, range from 0.5 h to 1000 h with a median of 10 h and 0.5 to 10 h with a median of 1 h, respectively (Boano et al., 2010; Gomez-Velez et al., 2015; Gomez et al., 2012; Pinay et al., 2009; Zarnetske et al., 2011). The lower bound of our representative BTSs was set to 1 h since reactions with BTS below 1 h are all very fast relative to the RTD, for which the form of distribution will make little difference. On the other hand, BTS larger than 1000 h was not explored because the exceeding probably of residence times beyond 1000 h is negligible. The fractions of consumed reactant with time $F_{solute}(t)$ of the four representative BTSs were compared with the overall CRTD in Figure 9. The values of BTSs and mean residence time were marked with black and red triangles, respectively. Based on the definition of

Damköhler number, our simulated HEFs were mass-transfer limited with lower BTSs (≤100h), then switched to a reaction rate limited system with higher BTSs (≥1000h).

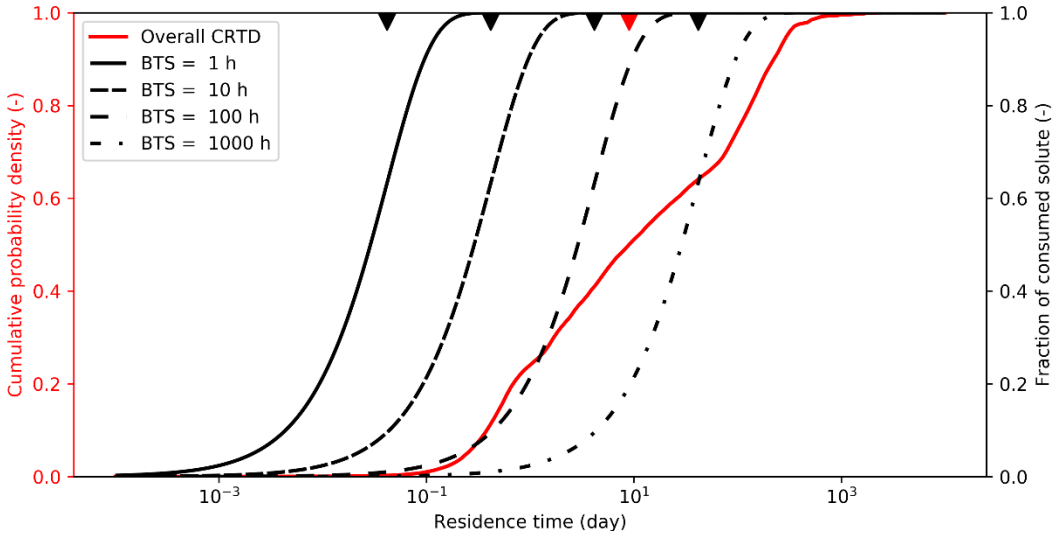

Figure 9. Fraction of consumed reactant under various BTSs (black lines) with the overall CRTD (red line). The red triangle maker indicates the mean residence time value, the black triangle markers indicate the BTS values.

The biogeochemical reaction potentials under different combination of RTDs and BTSs are illustrated by the predicted reactant consumptions (Figures 10-11). The simulated overall RTD (red solid lines) and the single-mode RTD (black dash lines) produced almost identical reactant consumption in a strongly mass-transfer limited (BTS<=10h, D>>10) system (e.g., Figure 10 a, b). The differences between the simulated RTD and the single-mode RTD became large when the Damköhler numbers were closer to one (BTS=100h, 1000h), but they were still less than 5% (e.g., Figures 10 c, d). It would be expected that their differences become smaller with a even smaller Damköhler number (D<<0.1) and the associated minimum reaction rates.

The biogeochemical impacts of RTD's temporal and spatial variations are revealed by the uncertain ranges of discrete RTDs (colored shadows in Figures 10-11). RTDs estimated from the smaller time windows produced markedly different reactant consumption profiles (the dark blue histograms in Figure 10 a-d). The uncertainty range of predicted reactant consumption reduced to less than ±20% when a full-year window of particles were included for the RTD estimations (the light blue histogram in Figure 10 i-l). The largest uncertainty of reactant consumptions appeared when the Damköhler numbers were close to one (Figures 10c, d, g, h, k, l). Our results also showed that the spatial uncertainty of the reactant consumption (Figure 11) was relatively small compared to its temporal counterpart (Figure 10), which is consistent with the smaller spatial variations of RTDs observed in section 3.4. It should be noted that we underestimated the spatial heterogeneity of reaction rates by applying universal BTSs to the entire reach. We did not account for large differences in microbial communities and associated reactions in two locations that were only 150 m apart as revealed in a previous study at the same site (Graham et al., 2018).

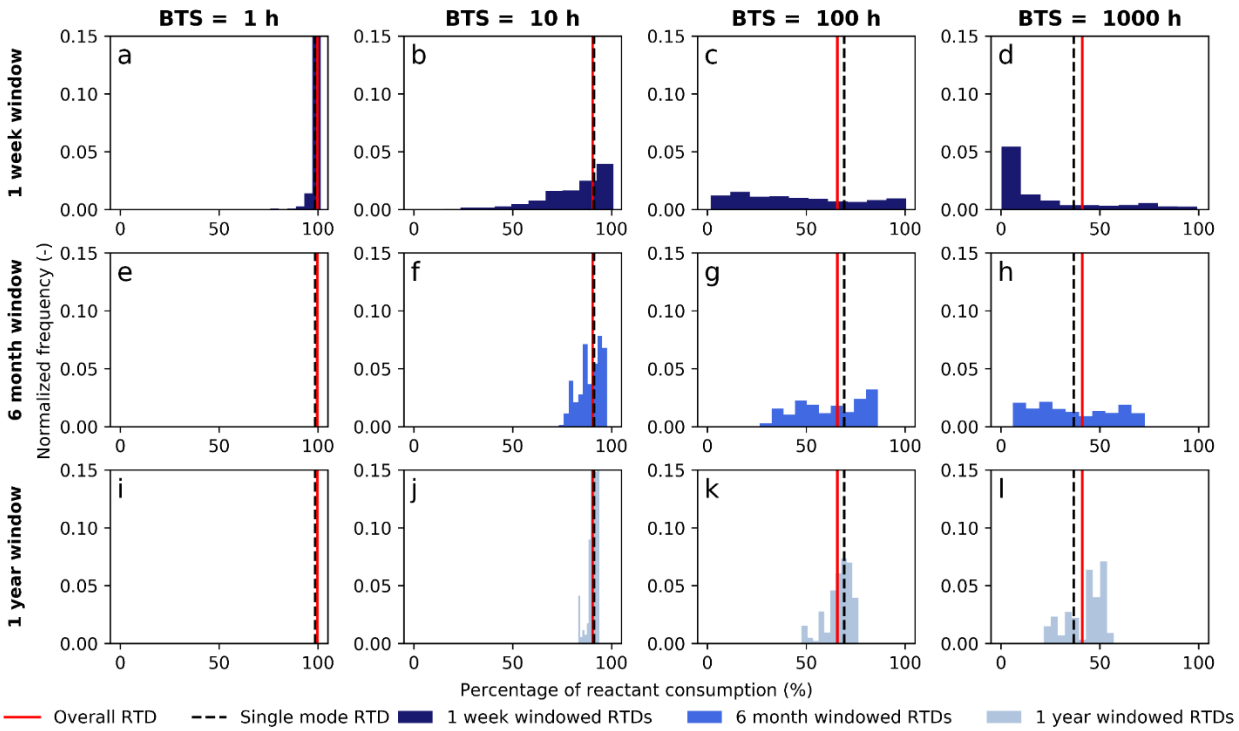

Figure 10. Prediction of reactant consumption with various BTSs and temporally discrete RTDs. Each column represent different BTS and each row represent RTDs from different temporal subsets of particals. The red solid lines are results from reactant consumption of the simulated overall RTDs, the black dash lines are results from fitted single mode RTDs.

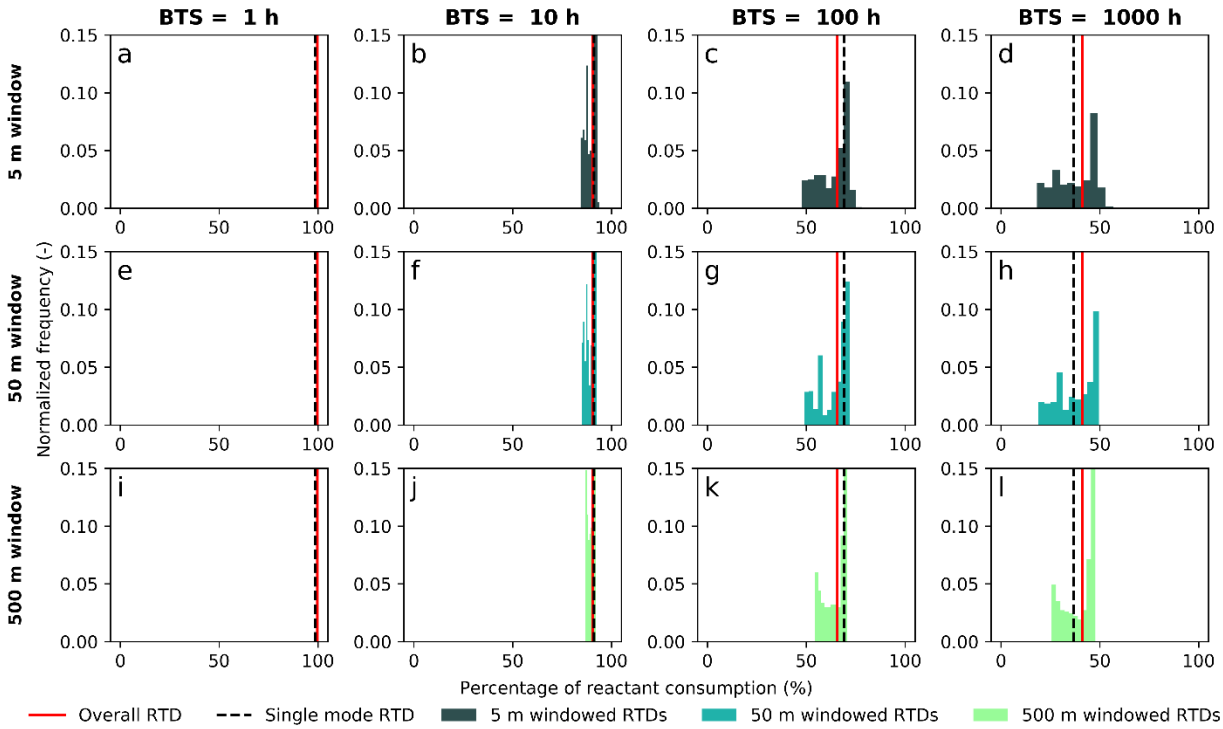

Figure 11. Prediction of reactant consumption with various BTSs and spatially discrete RTDs. Each column represent different BTS and each row represent RTDs from different spatial subsets of particles. The red solid lines are results from reactant consumption of the simulated RTDs, the black dash lines are results from fitted single mode RTDs.

3.6 Impacts of Dam-Induced High-Frequency Flow Variations on RTDs

One common characteristic of regulated river corridors is dam-induced, high-frequency flow variations. In a previous study (Song et al., 2018), it is found that upstream dam operations of the Hanford site for power production cause additional strong daily and weak weekly signals in river discharge and hydrograph. Here, we use moving average as a low pass filter to remove the sub-daily signal of river stage and groundwater data to create a new flow model with the smoothed flow boundaries (Figure 12a). This smoothed model was used to evaluate the effects of short-term river flow variations on the RTDs.

Comparison of the RTDs under the baseline case and smoothed case revealed an inherent correlation between the modes of RTDs and river stage variations. The fraction of short resident time components was dramatically reduced due to the removal of high-frequency river fluctuation in the smoothed case (Figure 12b). As a result, the high residence time components in the overall RTD of the smoothed case increased. Since the overall residence time increased in the smoothed case, the reactant had more time to react and the HEFs leaned towards a more reaction rate limited system. The smoothed case consumed more reactant than the baseline case among all BTSs, especially for the reactions with longer BTSs (Figure 12c). Since the total exchange flux of the baseline case is 127% of the smoothed case with the high-frequency flow variations, we further scaled the percentage of reactant consumption of the baseline case in Figure 12c by 1.27 to reflect the difference of hydrologic exchange. The results (Figure 12d) revealed that daily high-frequency flow variations could potentially induce 16%~27% more reactant consumption over the smoothed case with dam operations removed for BTSs lower than 10h. It is interesting to note that the impacts of increased exchange volume were almost offset by the decrease of the overall RTD in the baseline case compared to the smoothed case for BTSs larger than 100h. This means the dam operation has the larger impacts on the reactions with shorter BTSs such as aerobic respiration and has fewer impacts on the reactions with longer BTSs.

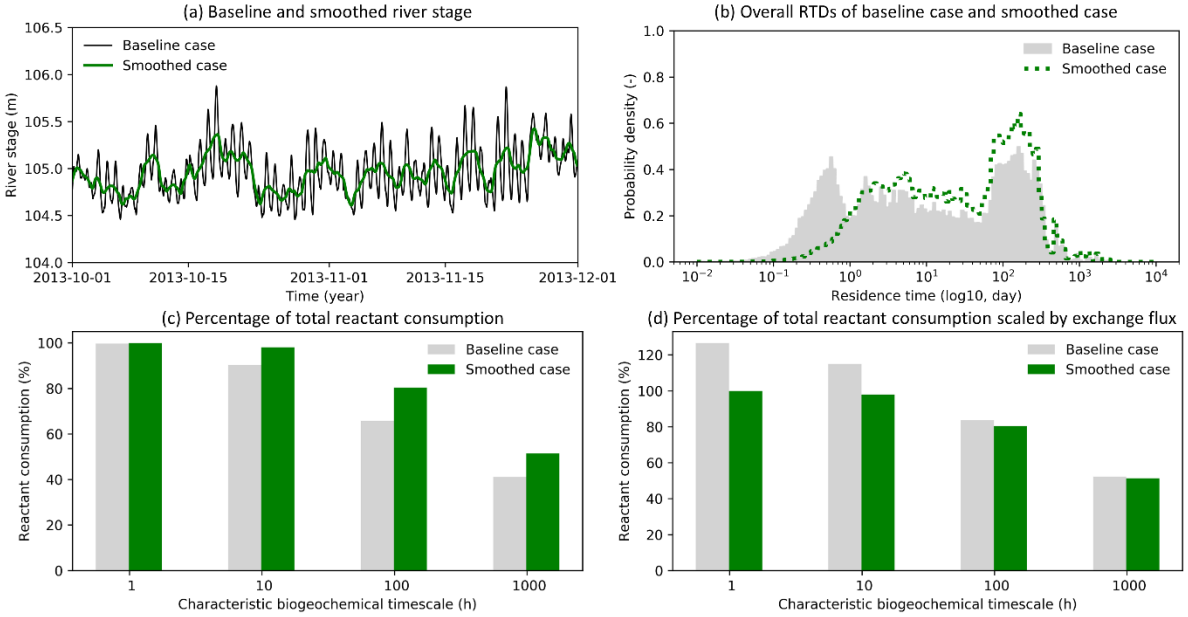

Figure 12. Impact of high-frequency flow variation on RTDs and biogeochemical reactions: a) baseline and smoothed river stage, b) simulated overall RTDs of baseline case and smoothed case, c) percentage of

total reactant consumption, and d) percentage of total reactant consumption scaled by exchange flux volume.

4. Discussions

4.1 Implication to Other Large River Corridors under Dynamic Flow Conditions

Our results demonstrate the significant contributions of lateral exchange flows in the HEFs of a gravel-bedded river system. The typical approach to evaluate HEFs at the large scale (reach to basin) is to develop surrogate models with modest requirements for 1) hydrologic and hydrogeologic data and 2) computational resources, such as the Networks with EXchange and Subsurface Storage (NEXSS) (Gomez-Velez & Harvey, 2014). These analytical or semi-analytical models often rely on steady-state flow conditions by assuming riverbed hyporheic exchange as the dominant exchange form in large river corridors. Using this approach, (Gomez-Velez et al., 2015) concluded that vertical hyporheic exchange is at least five times larger than the lateral hyporheic exchange in the Mississippi River network. Our simulations and observations revealed that highly dynamic river fluctuations could create significant lateral bank storage with a broader range of RTDs than previously reported (Kiel & Cardenas, 2014) because of the gravel-bedded nature of the Columbia River and corridor. The lateral exchange flows should be accounted for in the future development of river basin scale models for gravel-bedded systems.

Our simulated RTDs inherit the dynamic nature of river fluctuations. The impact of multi-frequency flow variations interacting with the complex subsurface stratigraphy led to temporally and spatially varied exchange patterns and RTDs. On one hand, the estimated RTDs from particle tracking had more long-term components in flood years and more short-time components in drought years. Thus the overall shape of the simulated RTDs depended strongly on the hydrological characteristics of the years being evaluated. On the other hand, the frequency of river fluctuations has a profound influence on the shape of RTDs. After removing the high-frequency fluctuations, the short-term components were significantly reduced with resulted increasing mean RTDs. For future studies in a regulated river, we suggest 1) including the river dynamic as one contributing factor in reduced-order models (e.g., NEXSS) and 2) using the dominated frequencies of river fluctuations as one guidance for in-situ experiment designs (e.g., determining the sampling frequency of tracer tests).

The single mode RTDs and associated mean RTDs are still valuable overall statistics for quantifying the biogeochemical impacts of RTDs in dynamic river systems. It is challenging to generate a universal multimodal RTD for different locations and periods in a given river reach, and even more so for different riverine systems. Despite that, we note that not all the modes of the multimodal RTDs have equal contributions to biogeochemical transformation. The number of long-term modes (e.g., more than one year) in the RTDs may be less critical since the transport scale will be long enough for most biogeochemical reactions to reach completion (Harvey et al., 2018). For the reactions with fast reaction rate (e.g., aerobic respiration), only first one or two modes impact reactant consumption. Thus, the impact of RTD multimodality at any given site will depend on the BTSs of its dominant reactions. We found that multimodality had the largest impact on biogeochemical reactions when the Damköhler number was close to one. The single mode approximation to the multimodal RTD yields equivalent predictions (<5% difference) of reactant consumption over the wide range of BTSs evaluated in this study. It seems a single-mode RTD assumption can be generally applied to a multimodal system without inducing excessive reactivity bias (e.g., 10%). However, it should be noted that uncertainty in the temperature dependence of reactions, rate constants, and associated functional microbial populations, and local vegetation (Graham et al., 2018) may produce even more significant uncertainty which is not accounted for in this study. Expanded investigations leveraging more field survey data to evaluate the rate variation in the same river reach and across many rivers would be valuable in future studies.

Dam-induced high-frequency stage fluctuations shorten the RTDs, which has significate impacts on biogeochemical processes in the HEFs. The influences of the high-frequency stage fluctuation on HEFs has been evaluated in several studies. High-frequency flow variations induce more flow reversals, higher

mass exchange, and deeper penetration depth of river thermal signals into the aquifer (Sawyer et al., 2009; Shuai et al., 2019; Song et al., 2018). The increased mass exchange might accelerate the subsurface reactions by providing more reactants (Song et al., 2018; Trauth & Fleckenstein, 2017) or decrease specific reactions by inducing strong inhibition (Knights et al., 2017). The response of biogeochemical reactions to stage fluctuation can be even more complicated if coupled with heterogeneous aquifer properties and thermal-dependent reactions (Song et al., 2018). By comparing the overall RTD of the baseline case and smoothed case, our results showed the high-frequency flow variation reduced the reaction rates by shortening the residence time, while the overall reactant consumption rose due to increased exchange volume. For reactions with longer reaction time scales (BTS>100h), the impacts of increased mass exchange was offset by the residence time reduction. It should be noted that the biogeochemical impacts of dam operation on arbitrary river systems can vary a lot according to distinct sediment properties, flow dynamics, and microbial community, etc. These results of dam-induced stage fluctuations have important implications for river management strategies that strive to optimize river biogeochemical function for maximum ecological services, riverine health, and water quality.

4.2 Limitations of this Study

There are limitations to our modeling approach that should be acknowledged. First, water flow through the alluvium was not directly modeled due to insufficient field measurements and the limitation of model resolution. Whereas the conductance boundary condition adopted in this study is an adequate approach to dampen river pulse propagation into the aquifer, it cannot represent the higher porosity (~0.4) of alluvium layer as compared to the Hanford Formation (~0.2). Pore velocity in the near-shore area was consequently overestimated by a factor of 2~3, artificially accelerating particle movements in the near-shore area. In addition, a uniform conductance value for the flow model was fit to capture the rising/falling trends of SpC measurements in the monitoring wells, but this was not a rigorous model calibration. The actual exchange flow pattern was undoubtedly more complicated with a heterogeneous riverbed permeability field that would lead to longer tailings of the RTDs.

Second, a simple first-order decay rate assumption was applied for the biogeochemical reactions. The actual transformations are far more complex, which usually involve various electron donors (e.g., carbon) and acceptors (e.g., oxygen and nitrate). Additionally, nonlinear interactions among reactions such as inhibition of aerobic respiration to denitrification may be significant. These sophisticated biogeochemical processes are not captured in the decay model used in our study.

Third, the smoothed case with a moving average was an estimation of the flow without dam operation, the impacts of dam operation might be overestimated since moving average removed all sub-daily frequency induced by both natural processes and anthropogenic activities.

Finally, the river channel geomorphology and hydrogeology also have strong controls on the locations of exchange hot spots and potentially RTDs (Shuai et al., 2019), which were not fully accounted in this study with the 1.6km river reach model. The influence of larger scale (10~100km scale) channel geomorphology, hydrogeology and also riverbed sediment heterogeneity (Hou et al., 2019) on RTDs will be addressed in our future work.

5. Conclusion

Dynamic flow variation is a common phenomenon in most large regulated rivers. Here, we used particle tracking to evaluate influences of river stage variations on RTDs, and their biogeochemical reaction potentials in the Hanford Reach under dam operations. Our results showed that river fluctuations created rapidly changing losing-gaining conditions between river and groundwater, which interacted with complex aquifer hydrogeological structure and led to complex exchange flow paths in the aquifer. This

study also demonstrated that RTDs of hydrological exchange flows can exhibit transient multimodal distributions as compared to the time-invariant RTDs commonly observed under steady flow conditions.

Analysis of RTDs from temporal and spatial subsets of particles showed that temporal river flow variation was the major contributor to multimodal RTDs. Statistical tests suggested that it may not be possible to determine a precise shape of RTDs in an aquifer with complex hydrogeological features under dynamic flow conditions. Thus it is needed to include river dynamics as one contributing factor in the assessment of RTDs in similar managed river corridors and development of reduced-order models in large scale (basin to watershed scale) studies. The simulations conducted under different flow conditions indicated that the frequency components of flow variation also had substantial impacts on the multimodal distribution of RTDs.

Our results also revealed that the multimodal characteristic of RTDs had a relatively small impact (<5%) on the computed extent of reactant consumption of representative biogeochemical reactions. Although the impacts of RTD multimodality at any given site will depend on the BTSs of its dominant reactions, our results suggested the largest deviation of the conventional single-mode assumption from the simulated multimodal RTDs appeared when the Damköhler number was close to one.

We found that high-frequency flow variations significantly altered the shape of RTDs and had a strong influence on river corridor biogeochemistry compared to that under the case without high-frequency flows. High-frequency flow variations created more short-time turnovers of exchange flow, which induced more exchange volume with shorter residence time. The impact of high-frequency flow variation on hyporheic biogeochemical reactions was found to be two-sided. The increased exchange volume brought more biogeochemical reactants to the hydrologic exchange zone, but the short residence time might not be sufficient for complete reaction. Our results indicated that the high-frequency flow variations generally increased biogeochemical transformations within HEFs, especially for reactions with higher rates. These finding have important ecological implications on how to maximize the potential benefits, or minimize the drawbacks, of river regulation to river ecosystems.

Acknowledgments

This paper describes objective technical results and analysis. Any subjective views or opinions that might be expressed in the paper do not necessarily represent the views of the U.S. Department of Energy or the United States Government. This research was supported by the U.S. Department of Energy (DOE), Office of Biological and Environmental Research (BER), as part of BER's Subsurface Biogeochemical Research Program (SBR). This research used resources of the National Energy Research Scientific Computing Center, a DOE Office of Science User Facility supported by the Office of Science of the U.S. Department of Energy under Contract No. DE-AC02-05CH11231. All the data used to produce the results in this study can be downloaded from https://osf.io/sy7at/.
Sandia National Laboratories is a multi-mission laboratory managed and operated by National Technology & Engineering Solutions of Sandia, LLC, a wholly owned subsidiary of Honeywell International Inc., for the U.S. Department of Energy's National Nuclear Security Administration under contract DE-NA0003525.

Reference

Arntzen, E. V., Geist, D. R., & Dresel, P. E. (2006). Effects of fluctuating river flow on groundwater/surface water mixing in the hyporheic zone of a regulated, large cobble bed river. *River Research and Applications*, *22*(8), 937–946. https://doi.org/10.1002/rra.947

Aubeneau, A. F., Martin, R. L., Bolster, D., Schumer, R., Jerolmack, D., & Packman, A. (2015). Fractal patterns in riverbed morphology produce fractal scaling of water storage times. *Geophysical*

Research Letters, *42*(13), 5309–5315. https://doi.org/10.1002/2015GL064155
Bekins, B. A., Warren, E., & Godsy, E. M. (1998). A comparison of zero-order, first-order, and monod biotransformation models. *Ground Water*. https://doi.org/10.1111/j.1745-6584.1998.tb01091.x
Bjornstad, B. N., Horner, J. A., Vermeul, V. R., Lanigan, D. C., & Thorne, P. D. (2009). *Borehole Completion and Conceptual Hydrogeologic Model for the IFRC Well Field, 300 Area, Hanford Site*. Richland, WA (United States). https://doi.org/10.2172/974984
Boano, F., Demaria, A., Revelli, R., & Ridolfi, L. (2010). Biogeochemical zonation due to intrameander hyporheic flow. *Water Resources Research*, *46*(2). https://doi.org/10.1029/2008WR007583
Boano, F., Harvey, J. W. W., Marion, A., Packman, a. I. I., Revelli, R., Ridolfi, L., & Wörman, A. (2014). Hyporheic flow and transport processes: Mechanisms, models, and biogeochemical implications. *Reviews of Geophysics*, *52*(4), 603–679. https://doi.org/10.1002/2012RG000417
Botter, G., Bertuzzo, E., & Rinaldo, A. (2011). Catchment residence and travel time distributions: The master equation. *Geophysical Research Letters*, *38*(11), 1–6. https://doi.org/10.1029/2011GL047666
Boulton, A. J., Findlay, S., Marmonier, P., Stanley, E. H., & Valett, H. M. (1998). THE FUNCTIONAL SIGNIFICANCE OF THE HYPORHEIC ZONE IN STREAMS AND RIVERS. *Annual Review of Ecology and Systematics*, *29*(1), 59–81. https://doi.org/10.1146/annurev.ecolsys.29.1.59
Briggs, M. A., Lautz, L. K., & Hare, D. K. (2014). Residence time control on hot moments of net nitrate production and uptake in the hyporheic zone. *Hydrological Processes*, *28*(11), 3741–3751. https://doi.org/10.1002/hyp.9921
Briody, A. C., Cardenas, M. B., Shuai, P., Knappett, P. S. K., & Bennett, P. C. (2016). Groundwater flow, nutrient, and stable isotope dynamics in the parafluvial-hyporheic zone of the regulated Lower Colorado River (Texas, USA) over the course of a small flood. *Hydrogeology Journal*, *24*(4), 923–935. https://doi.org/10.1007/s10040-016-1365-3
Buffington, J. M., & Tonina, D. (2009). Hyporheic exchange in mountain rivers II: Effects of channel morphology on mechanics, scales, and rates of exchange. *Geography Compass*. https://doi.org/10.1111/j.1749-8198.2009.00225.x
Cardenas, M. B. (2008). Surface water-groundwater interface geomorphology leads to scaling of residence times. *Geophysical Research Letters*, *35*(8), L08402. https://doi.org/10.1029/2008GL033753
Cardenas, M. B. (2015). Hyporheic zone hydrologic science: A historical account of its emergence and a prospectus. *Water Resources Research*, *51*(5), 3601–3616. https://doi.org/10.1002/2015WR017028
Cardenas, M. B., & Wilson, J. L. (2007). Dunes, turbulent eddies, and interfacial exchange with permeable sediments. *Water Resources Research*, *43*(8). https://doi.org/10.1029/2006WR005787
Cardenas, M. B., Wilson, J. L., & Zlotnik, V. A. (2004). Impact of heterogeneity, bed forms, and stream curvature on subchannel hyporheic exchange. *Water Resources Research*, *40*(8), 1–14. https://doi.org/10.1029/2004WR003008
Chen, X., Murakami, H., Hahn, M. S., Hammond, G. E., Rockhold, M. L., Zachara, J. M., & Rubin, Y. (2012). Three-dimensional Bayesian geostatistical aquifer characterization at the Hanford 300 Area using tracer test data. *Water Resources Research*, *48*(6), 1–20. https://doi.org/10.1029/2011WR010675
Chen, X., Hammond, G. E., Murray, C. J., Rockhold, M. L., Vermeul, V. R., & Zachara, J. M. (2013). Application of ensemble-based data assimilation techniques for aquifer characterization using tracer data at Hanford 300 area. *Water Resources Research*, *49*(10), 7064–7076. https://doi.org/10.1002/2012WR013285
Faulkner, B. R., Renée Brooks, J., Forshay, K. J., & Cline, S. P. (2012). Hyporheic flow patterns in relation to large river floodplain attributes. *Journal of Hydrology*, *448–449*, 161–173. https://doi.org/10.1016/j.jhydrol.2012.04.039
Fayer, M. J., & Walters, T. B. (1995). *Estimated recharge rates at the Hanford Site*. *Acta Geophysica Polonica* (Vol. v 53, n SP). Richland, WA. https://doi.org/10.2172/10122247
van Genuchten, M. T. (1980). A Closed-form Equation for Predicting the Hydraulic Conductivity of Unsaturated Soils1. *Soil Science Society of America Journal*, *44*(5), 892.

https://doi.org/10.2136/sssaj1980.03615995004400050002x

Gomez-Velez, J. D., Wilson, J. L., Cardenas, M. B., & Harvey, J. W. (2017). Flow and Residence Times of Dynamic River Bank Storage and Sinuosity-Driven Hyporheic Exchange. *Water Resources Research*, *53*(10), 8572–8595. https://doi.org/10.1002/2017WR021362

Gomez-Velez, Jesus D., & Harvey, J. W. (2014). A hydrogeomorphic river network model predicts where and why hyporheic exchange is important in large basins. *Geophysical Research Letters*. https://doi.org/10.1002/2014GL061099

Gomez-Velez, Jesus D., Harvey, J. W., Cardenas, M. B., & Kiel, B. (2015). Denitrification in the Mississippi River network controlled by flow through river bedforms. *Nature Geoscience*, *8*(12), 941–945. https://doi.org/10.1038/ngeo2567

Gomez, J. D., & Wilson, J. L. (2013). Age distributions and dynamically changing hydrologic systems: Exploring topography-driven flow. *Water Resources Research*, *49*(3), 1503–1522. https://doi.org/10.1002/wrcr.20127

Gomez, Jesus D., Wilson, J. L., & Cardenas, M. B. (2012). Residence time distributions in sinuosity-driven hyporheic zones and their biogeochemical effects. *Water Resources Research*, *48*(9). https://doi.org/10.1029/2012WR012180

Graf, W. L. (1999). Dam nation: A geographic census of American dams and their large-scale hydrologic impacts. *Water Resources Research*, *35*(4), 1305–1311. https://doi.org/10.1029/1999WR900016

Graham, E. B., Crump, A. R., Kennedy, D. W., Arntzen, E., Fansler, S., Purvine, S. O., et al. (2018). Multi 'omics comparison reveals metabolome biochemistry, not microbiome composition or gene expression, corresponds to elevated biogeochemical function in the hyporheic zone. *Science of the Total Environment*, *642*, 742–753. https://doi.org/10.1016/j.scitotenv.2018.05.256

Haggerty, R., Wondzell, S. M., & Johnson, M. A. (2002). Power-law residence time distribution in the hyporheic zone of a 2nd-order mountain stream. *Geophysical Research Letters*, *29*(13). https://doi.org/10.1029/2002GL014743

Hammond, G. E., Lichtner, P. C., & Mills, R. T. (2014). Evaluating the performance of parallel subsurface simulators: An illustrative example with PFLOTRAN. *Water Resources Research*, *50*(1), 208–228. https://doi.org/10.1002/2012WR013483

Hammond, Glenn E., & Lichtner, P. C. (2010). Field-scale model for the natural attenuation of uranium at the Hanford 300 Area using high-performance computing. *Water Resources Research*, *46*(9). https://doi.org/10.1029/2009WR008819

Harman, C. J., Ward, A. S., & Ball, A. (2016). How does reach-scale stream-hyporheic transport vary with discharge? Insights from rSAS analysis of sequential tracer injections in a headwater mountain stream. *Water Resources Research*, *52*(9), 7130–7150. https://doi.org/10.1002/2016WR018832

Harvey, J., & Gooseff, M. (2015). River corridor science: Hydrologic exchange and ecological consequences from bedforms to basins. *Water Resources Research*, *51*(9), 6893–6922. https://doi.org/10.1002/2015WR017617

Harvey, J., Gomez-Velez, J., Schmadel, N., Scott, D., Boyer, E., Alexander, R., et al. (2018). How Hydrologic Connectivity Regulates Water Quality in River Corridors. *Journal of the American Water Resources Association*, *55*(2), 369–381. https://doi.org/10.1111/1752-1688.12691

Harvey, J. W., Böhlke, J. K., Voytek, M. A., Scott, D., & Tobias, C. R. (2013). Hyporheic zone denitrification: Controls on effective reaction depth and contribution to whole-stream mass balance. *Water Resources Research*, *49*(10), 6298–6316. https://doi.org/10.1002/wrcr.20492

Hou, Z., Scheibe, T. D., Murray, C. J., Perkins, W. A., Arntzen, E. V., Ren, H., et al. (2019). Identification and mapping of riverbed sediment facies in the Columbia River through integration of field observations and numerical simulations. *Hydrological Processes*, *33*(8), 1245–1259. https://doi.org/10.1002/hyp.13396

Jonsson, K., Johansson, H., & Wörman, A. (2003). Hyporheic exchange of reactive and conservative solutes in streams - Tracer methodology and model interpretation. *Journal of Hydrology*, *278*(1–4), 153–171. https://doi.org/10.1016/S0022-1694(03)00140-9

Kiel, B. A., & Bayani Cardenas, M. (2014). Lateral hyporheic exchange throughout the Mississippi River

738 network. *Nature Geoscience*. https://doi.org/10.1038/ngeo2157
739 Knapp, J. L. A., González-Pinzón, R., Drummond, J. D., Larsen, L. G., Cirpka, O. A., & Harvey, J. W.
740 (2017). Tracer-based characterization of hyporheic exchange and benthic biolayers in streams.
741 *Water Resources Research*, *53*(2), 1575–1594. https://doi.org/10.1002/2016WR019393
742 Knights, D., Sawyer, A. H., Barnes, R. T., Musial, C. T., & Bray, S. (2017). Tidal controls on riverbed
743 denitrification along a tidal freshwater zone. *Water Resources Research*, *53*(1), 799–816.
744 https://doi.org/10.1002/2016WR019405
745 Larsen, L. G. G., Harvey, J. W. W., & Maglio, M. M. M. (2014). Dynamic hyporheic exchange at
746 intermediate timescales: Testing the relative importance of evapotranspiration and flood pulses.
747 *Water Resources Research*, *50*(1), 318–335. https://doi.org/10.1002/2013WR014195
748 Liu, S., & Chui, T. F. M. (2018). Impacts of Streambed Heterogeneity and Anisotropy on Residence Time
749 of Hyporheic Zone. *Groundwater*, *56*(3), 425–436. https://doi.org/10.1111/gwat.12589
750 McCallum, J. L., & Shanafield, M. (2016). Residence times of stream-groundwater exchanges due to
751 transient stream stage fluctuations. *Water Resources Research*, *52*(3), 2059–2073.
752 https://doi.org/10.1002/2015WR017441
753 Neitzel, D. A., Antonio, E. J., Eschbach, T. O., Fowler, R. A., Goodwin, S. M., Harvey, D. W., et al.
754 (2001). *Hanford Site National Environmental Policy Act (NEPA) Characterization*. Richland, WA
755 (United States): Pacific Northwest National Laboratory (PNNL), Richland, WA (US).
756 https://doi.org/10.2172/789446
757 Nilsson, C., Reidy, C. A., Dynesius, M., & Revenga, C. (2005). Fragmentation and flow regulation of the
758 world's large river systems. *Science*, *308*(5720), 405–408. https://doi.org/10.1126/science.1107887
759 Pinay, G., O'Keefe, T. C., Edwards, R. T., & Naiman, R. J. (2009). Nitrate removal in the hyporheic zone
760 of a salmon river in Alaska. *River Research and Applications*. https://doi.org/10.1002/rra.1164
761 Pollock, D. W. (1994). *User's Guide for MODPATH/MODPATH-PLOT, Version 3: A particle tracking*
762 *post-processing package for MODFLOW, the U.S. Geological Survey finite-difference ground-water*
763 *flow model* (Open-File Report). *Open-File Report 94-464*. https://doi.org/94-464
764 Richmond, M. C., & Perkins, W. A. (2009). Efficient calculation of dewatered and entrapped areas using
765 hydrodynamic modeling and GIS. *Environmental Modelling and Software*, *24*(12), 1447–1456.
766 https://doi.org/10.1016/j.envsoft.2009.06.001
767 Rinaldo, A., Benettin, P., Harman, C. J., Hrachowitz, M., McGuire, K. J., van der Velde, Y., et al. (2015).
768 Storage selection functions: A coherent framework for quantifying how catchments store and release
769 water and solutes. *Water Resources Research*, *51*(6), 4840–4847.
770 https://doi.org/10.1002/2015WR017273
771 Salehin, M., Packman, A. I., & Paradis, M. (2004). Hyporheic exchange with heterogeneous streambeds:
772 Laboratory experiments and modeling. *Water Resources Research*.
773 https://doi.org/10.1029/2003WR002567
774 Sawyer, A. H., & Cardenas, M. B. (2009). Hyporheic flow and residence time distributions in
775 heterogeneous cross-bedded sediment. *Water Resources Research*, *45*(8), 1–12.
776 https://doi.org/10.1029/2008WR007632
777 Sawyer, A. H., Cardenas, M. B., Bomar, A., & Mackey, M. (2009). Impact of dam operations on
778 hyporheic exchange in the riparian zone of a regulated river. In *Hydrological Processes*.
779 https://doi.org/10.1002/hyp.7324
780 Schmadel, N. M., Ward, A. S., Lowry, C. S., & Malzone, J. M. (2016). Hyporheic exchange controlled by
781 dynamic hydrologic boundary conditions. *Geophysical Research Letters*, *43*(9), 4408–4417.
782 https://doi.org/10.1002/2016GL068286
783 Schmadel, N. M., Ward, A. S., & Wondzell, S. M. (2017). Hydrologic controls on hyporheic exchange in
784 a headwater mountain stream. *Water Resources Research*, *53*(7), 6260–6278.
785 https://doi.org/10.1002/2017WR020576
786 Shuai, P., Cardenas, M. B., Knappett, P. S. K., Bennett, P. C., & Neilson, B. T. (2017). Denitrification in
787 the banks of fluctuating rivers: The effects of river stage amplitude, sediment hydraulic conductivity
788 and dispersivity, and ambient groundwater flow. *Water Resources Research*, *53*(9), 7951–7967.

https://doi.org/10.1002/2017WR020610
Shuai, P., Chen, X., Song, X., Hammond, G. E., Zachara, J., Royer, P., et al. (2019). Dam Operations and Subsurface Hydrogeology Control Dynamics of Hydrologic Exchange Flows in a Regulated River Reach. *Water Resources Research*, 2018WR024193. https://doi.org/10.1029/2018WR024193
Song, X., Chen, X., Stegen, J., Hammond, G., Song, H., Dai, H., et al. (2018). Drought Conditions Maximize the Impact of High-Frequency Flow Variations on Thermal Regimes and Biogeochemical Function in the Hyporheic Zone. *Water Resources Research*, *54*(10), 7361–7382. https://doi.org/10.1029/2018WR022586
Spiegelhalter, D. J., Best, N. G., Carlin, B. P., & van der Linde, A. (2002). Bayesian measures of model complexity and fit. *Journal of the Royal Statistical Society: Series B (Statistical Methodology)*, *64*(4), 583–639. https://doi.org/10.1111/1467-9868.00353
Stegen, J. C., Johnson, T., Fredrickson, J. K., Wilkins, M. J., Konopka, A. E., Nelson, W. C., et al. (2018). Influences of organic carbon speciation on hyporheic corridor biogeochemistry and microbial ecology. *Nature Communications*, *9*(1), 585. https://doi.org/10.1038/s41467-018-02922-9
Stonedahl, S. H., Harvey, J. W., & Packman, A. I. (2013). Interactions between hyporheic flow produced by stream meanders, bars, and dunes. *Water Resources Research*. https://doi.org/10.1002/wrcr.20400
Tonina, D., & Buffington, J. M. (2011). Effects of stream discharge, alluvial depth and bar amplitude on hyporheic flow in pool-riffle channels. *Water Resources Research*, *47*(8), 1–13. https://doi.org/10.1029/2010WR009140
Trauth, N., & Fleckenstein, J. H. (2017). Single discharge events increase reactive efficiency of the hyporheic zone. *Water Resources Research*, *53*(1), 779–798. https://doi.org/10.1002/2016WR019488
Ward, A. S., Schmadel, N. M., & Wondzell, S. M. (2018). Time-Variable Transit Time Distributions in the Hyporheic Zone of a Headwater Mountain Stream. *Water Resources Research*, *54*(3), 2017–2036. https://doi.org/10.1002/2017WR021502
Williams, M. D., Rockhold, M. L., Thorne, P. D., & Chen, Y. (2008). *Three-Dimensional Groundwater Models of the 300 Area at the Hanford Site, Washington State*. *PNNL*. Richland, WA (United States). https://doi.org/10.2172/969184
Worman, A., Packman, A. I., Johansson, H. H., Jonsson, K., Wörman, A., Packman, A. I., et al. (2002). Effect of flow-induced exchnage in hyporheic zones on longitudinal transport of solutes in streams and rivers. *Water Resources Research*, *38*(1), 1–15. https://doi.org/10.1029/2001WR000769
Wörman, A., Packman, A. I., Marklund, L., Harvey, J. W., & Stone, S. H. (2007). Fractal topography and subsurface water flows from fluvial bedforms to the continental shield. *Geophysical Research Letters*, *34*(7), L07402. https://doi.org/10.1029/2007GL029426
Zachara, J. M., Long, P. E., Bargar, J., Davis, J. A., Fox, P., Fredrickson, J. K., et al. (2013). Persistence of uranium groundwater plumes: Contrasting mechanisms at two DOE sites in the groundwater-river interaction zone. *Journal of Contaminant Hydrology*, *147*, 45–72. https://doi.org/10.1016/j.jconhyd.2013.02.001
Zachara, J. M., Chen, X., Murray, C., & Hammond, G. (2016). River stage influences on uranium transport in a hydrologically dynamic groundwater-surface water transition zone. *Water Resources Research*, *52*(3), 1568–1590. https://doi.org/10.1002/2015WR018009
Zarnetske, J. P., Haggerty, R., Wondzell, S. M., & Baker, M. A. (2011). Dynamics of nitrate production and removal as a function of residence time in the hyporheic zone. *Journal of Geophysical Research*, *116*(G1), G01025. https://doi.org/10.1029/2010JG001356
Zhou, T., Bao, J., Huang, M., Hou, Z., Arntzen, E., Song, X., et al. (2018). Riverbed Hydrologic Exchange Dynamics in a Large Regulated River Reach. *Water Resources Research*, *54*(4), 2715–2730. https://doi.org/10.1002/2017WR020508

Water Resources Research
Supporting Information for

Controls of River Dynamics on Residence Time and Biogeochemical Reactions of Hydrological Exchange Flows in A Regulated River Reach

Xuehang Song[1], Xingyuan Chen[1,*], John M. Zachara[1], Jesus D. Gomez-Velez[2], Pin Shuai[1], Huiying Ren[1], and Glenn E Hammond[3]

[1]Pacific Northwest National Laboratory, Richland, Washington, USA.
[2]Civil & Environmental Engineering, Vanderbilt University, Nashville, Tennessee, USA.
[3]Applied Systems Analysis and Research, Sandia National Laboratories, Albuquerque, New Mexico, USA.

Contents of this file

Additional Supporting Information (Files uploaded separately)

Movie S1. Animation of pathlines of representative particles

Introduction

This supplementary information contains 1) governing equations of flow and solute transport; 2) particle tracking codes; 3) comparisons between simulated groundwater level and measured groundwater level; 4) snapshots of flow and tracer simulations.

Text S1

The governing flow equation in PFLOTRAN is based on the Richards equation

$$\frac{\partial(\rho s\varphi)}{\partial t} + \nabla\cdot(\rho q) = Q_w\,, \tag{S1}$$

with water density ρ, porosity φ, water saturation s, time t, and water source/sink Q_w. The Darcy velocity q is calculated by

$$q = -\frac{kk_r}{\mu}\nabla(p-\rho gz)\,, \tag{S2}$$

with liquid pressure p, intrinsic permeability k, relative permeability k_r, viscosity μ, gravitational acceleration g, and elevation z. For unsaturated flow, the van Genuchten model (van Genuchten, 1980) is used to relate capillary pressure to water saturation, and the Burdine relation (Burdine, 1953) is used for the relative permeability function.

The reactive transport processes include advection, dispersion, diffusion, and reactions with the following governing equation for a given species,

$$\frac{\partial(s\varphi C_i)}{\partial t} + \nabla \cdot (qC - \varphi sD\nabla C_i) = S_i + r_i \,, \tag{S3}$$

where C_i is the aqueous solute concentration, S_i is the source and sink term for the solute, r_i is the reaction rate. D is the effective dispersion coefficient that represents combined effects of molecular diffusion and microdispersion. Molecular diffusion is neglected in this case because of its small contribution compared to the dominating macrodispersion in this highly heterogeneous aquifer.

PFLOTRAN uses finite volume techniques to discretize the flow and transport partial differential equations (see (Glenn E. Hammond & Lichtner, 2010) and PFLOTRAN user guide https://www.pflotran.org/ for more details of the numerical scheme of PFLOTRAN). A variant of seepage boundary condition, so called "conductance boundary condition", is provided in PFLOTRAN for representing the thin low-permeability alluvium layer on top of the riverbed. In a model using structured mesh with finite volume representation, the boundary flux at an exterior face *b* of the boundary cell *n* is given by

$$F_{nb} = -\rho_{nb}\left(\frac{kk_r}{\mu}\right)_{nb}\left(\frac{P_b - P_n - \rho_{nb} g z_{nb}}{d_{nb}}\right), \tag{S4}$$

where P_b and P_n are the pressures at the face and cell center, respectively, and d_{nb} is the distance between the face and cell center. The permeablity at the river boundary is set to the value

$$k_{nb} = Cd_{nb} \,, \tag{S5}$$

Where the quantity C is referred to as the boundary conductance coefficient. The immplementation of conductance coeffient allows us to specifc the very thin low permeablity layer using half length of the boundary cells (0.25~2m in this study) (Glenn E. Hammond & Lichtner, 2010). Since the conductance coefficient has a dominant effect on the river stage fluctuation, it was selected as the main tuning parameter for better matches between simulated and observed groundwater level and tracer concentration data.

Text S2

A classical semi-analytical particle tracking scheme (Pollock, 1994) was adopted in this study, which tracks particles from one cell to the next with the assumption that flow is steady within given time step (1h in this study). Based on this algorithm, we developed a parallel version of particle tracking tool for PFLOTRAN that can track millions of particles simultaneously on clusters. The codes are open sourced and available online (https://github.com/xuehangsong/particle_tracking/tree/master/para). The particle tracking of this study was conducted on the KNL nodes of the National Energy Research Scientific Computing Center (NERSC), which took 48 hours with 680 cores and produced 10TB of pathline data. Figure S1 shows the flowchart of our particle tracking Python codes (see (Pollock, 1994) for more details of the particle tracking algorithm).

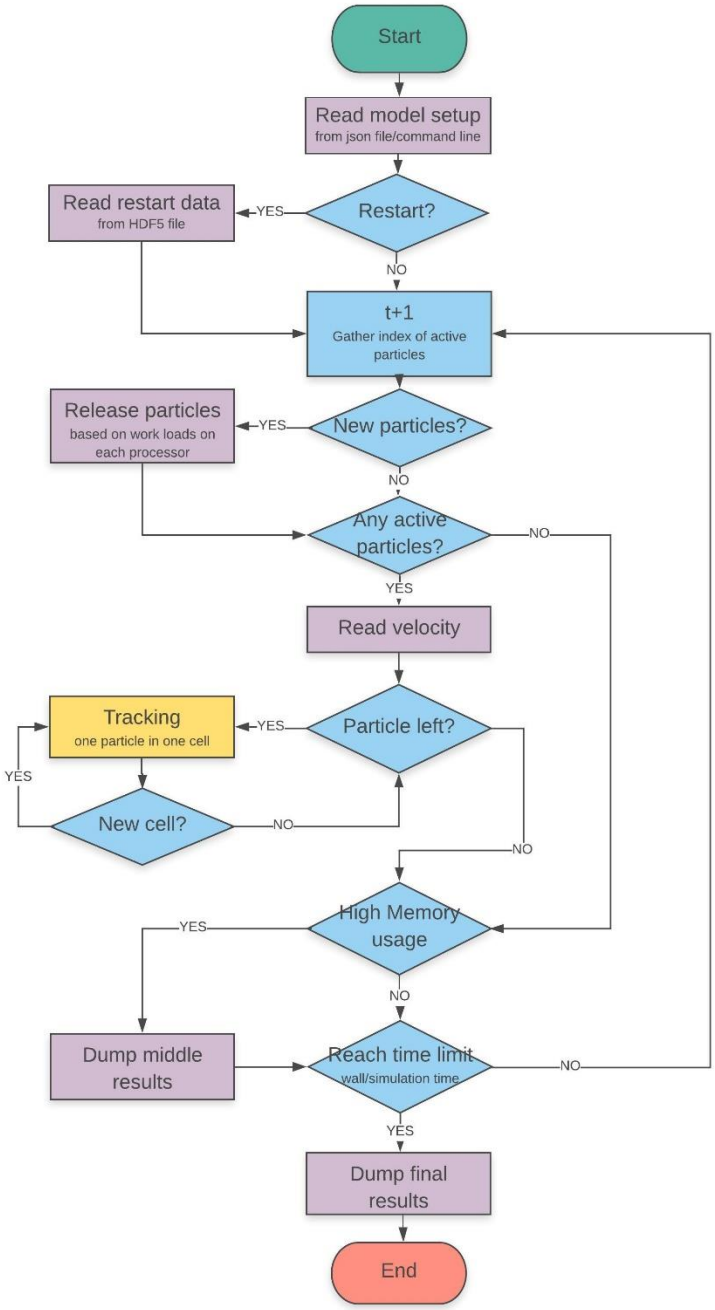

Figure S1. Flow chart of the particle tracking codes, the green block indicates program starting position, red block indicates program ending position, purple blocks are the IO processes, blue blocks are related to program flow control, and yellow block is the tracking algorithm.

Text S3

The simulated groundwater levels agreed well with the measured groundwater tables in the monitored wells as shown in the one to one scatter plots (Figure S2). There're minimum differences among the four different conductance cases due to the small hydraulic gradients of the highly permeable aquifer and well defined kriged boundaries.

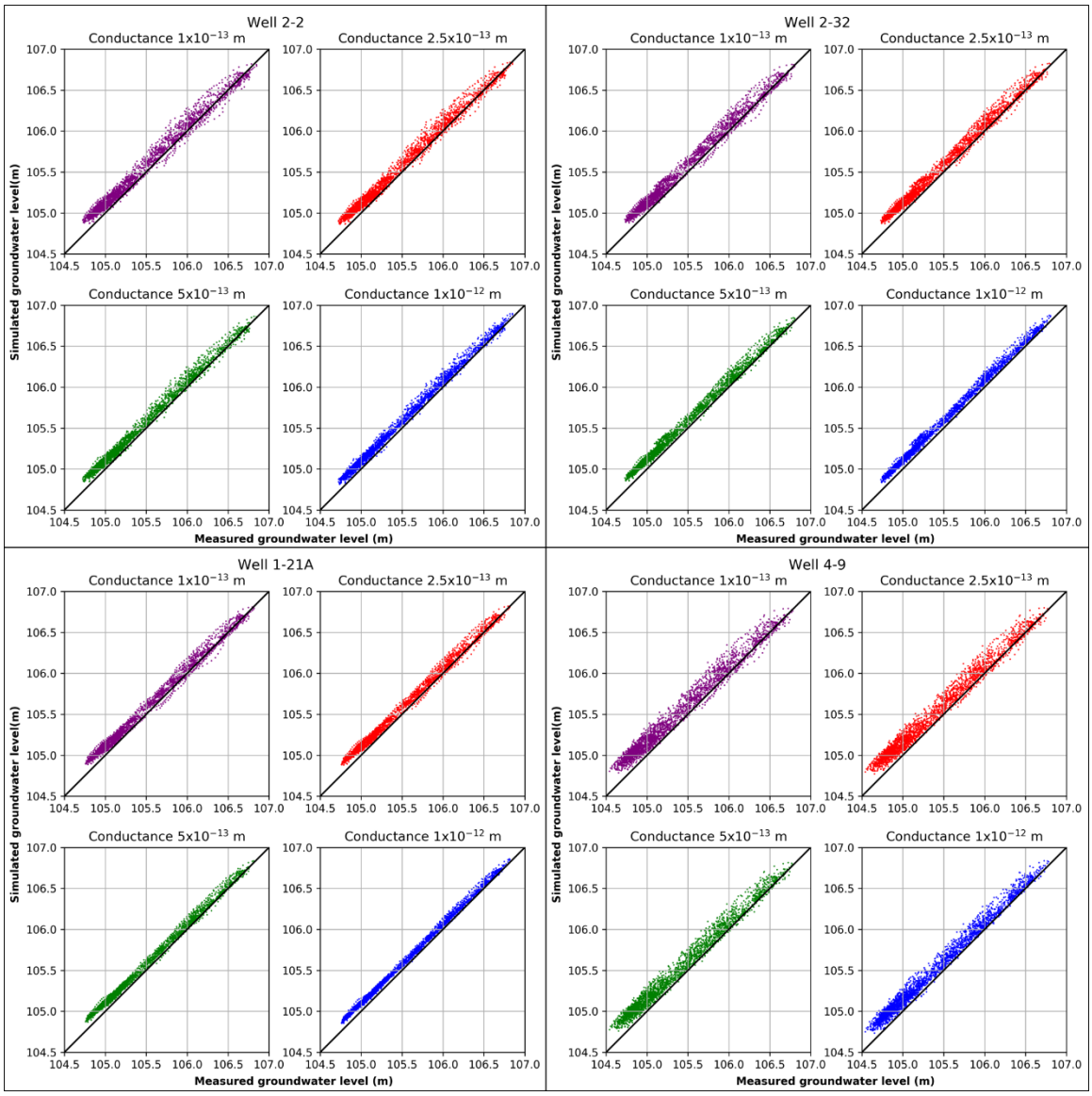

Figure S2. Comparison between simulated and observed groundwater level. Different colored dots represent different conductance values, the blank lines are identity lines.

Text S4

The simulated river intrusion are exhibited using simulated conservative tracer results in Figure S2. We selected three representative flow fields in an average flow year (2013), including river losing (T1 in Figure S2), river gaining (T3 in Figure S2) and neutral conditions (T2 in Figure S2). It should be noted the

simulated flow field was highly dynamic, and the exchange flow directions can easily be reversed within several hours due to river fluctuation.

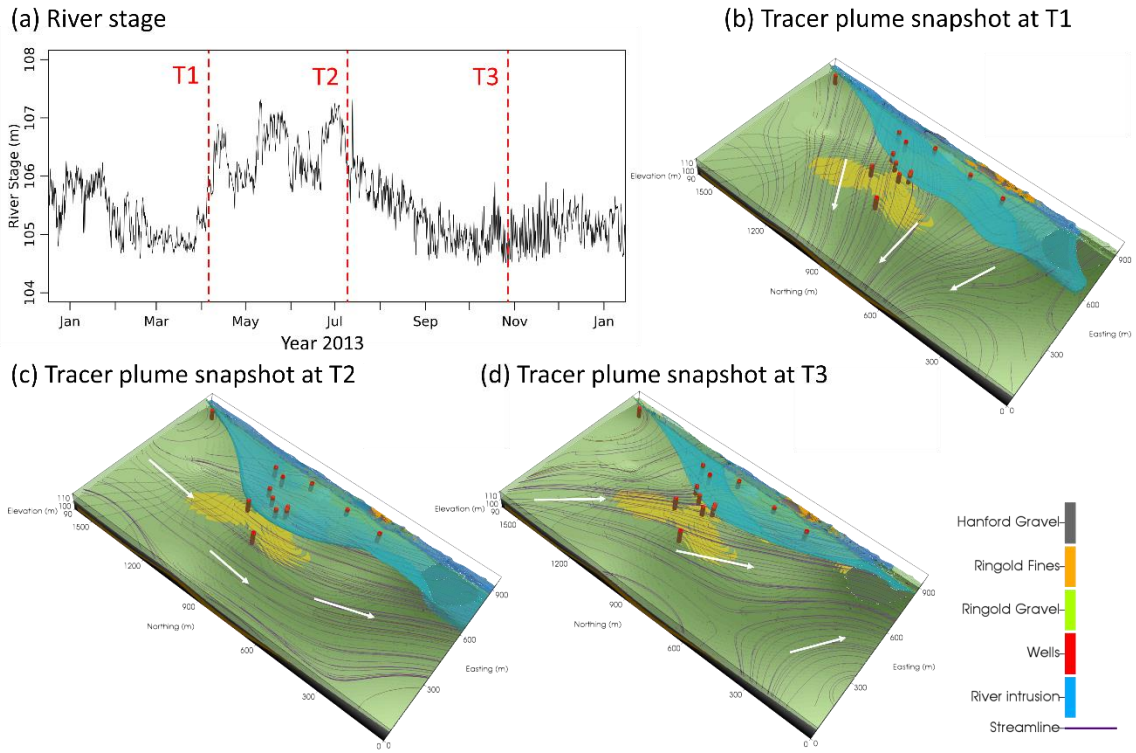

Figure S3. Simulated river water intrusion patterns. The upper Hanford Gravel (green) is set translucent to show the lower Ringold Fines (black) and Ringold Gravel (orange). The red cylinders represent the long-term monitoring groundwater wells used for model validation. The blue plumes represent subsurface waters with more than 50% river water. The streamline (purple lines) and flow directions (white arrow) were also plotted along with the tracer plume. (The plots was rotated 90 degrees in anticlockwise direction from Figure 2 in main text to better show the river intrusion).

Text S5

An animation of particle tracking is uploaded separately (Movie_S1.avi).